10.1161/CIRCULATIONAHA.117.033249

Defective Base Excision Repair of Oxidative DNA Damage in Vascular Smooth Muscle Cells Promotes Atherosclerosis

Running Title: *Shah et al.; Defective BER Promotes Atherosclerosis*

Aarti Shah, PhD[1]; Kelly Gray, PhD[1†]; Nichola Figg[1]; Alison Finigan[1]; Lakshi Starks[1]; Martin Bennett, MD, PhD[1*]

[1]Division of Cardiovascular Medicine, University of Cambridge, Addenbrooke's Centre for Clinical Investigation, Addenbrooke's Hospital, Cambridge, UK

[†]Present address: Cardiovascular Safety, AstraZeneca, Cambridge, UK

***Address for Correspondence:**
Martin Bennett, MD, PhD
Division of Cardiovascular Medicine
University of Cambridge
Addenbrooke's Centre for Clinical Investigation
Addenbrooke's Hospital
Cambridge, CB2 0QQ, UK
Tel: +44 1223 331504
Fax: +44 1223 331504
Email: mrb@mole.bio.cam.ac.uk

Abstract

***Background*—**Atherosclerotic plaques demonstrate extensive accumulation of oxidative DNA damage, predominantly as 8-oxoguanine (8oxoG) lesions. 8oxoG is repaired by base excision repair (BER) enzymes; however, the mechanisms regulating 8oxoG accumulation in vascular smooth muscle cells (VSMCs) and its effects on their function and in atherosclerosis are unknown.

***Methods*—**We studied levels of 8oxoG and its regulatory enzymes in human atherosclerosis, the mechanisms regulating 8oxoG repair and the BER enzyme 8oxoG DNA glycosylase I (OGG1) in VSMCs in vitro, and the effects of reducing 8oxoG in VSMCs in atherosclerosis in $ApoE^{-/-}$ mice.

***Results*—**Human plaque VSMCs showed defective nuclear 8oxoG repair, associated with reduced acetylation of OGG1. OGG1 was a key regulatory enzyme of 8oxoG repair in VSMCs, and its acetylation was crucial to its repair function, through regulation of protein stability and expression. p300 and SIRT1 were identified as the OGG1 acetyltransferase and deacetylase regulators respectively, and both proteins interacted with OGG1 and regulated OGG1 acetylation at endogenous levels. However, p300 levels were decreased in human plaque VSMCs and in response to oxidative stress, suggesting that ROS-induced regulation of OGG1 acetylation could be due to ROS-induced decrease in p300 expression. We generated mice that express VSMC-restricted OGG1 or an acetylation defective version (SM22α-OGG1 and SM22α-$OGG1^{K-R}$ mice) and crossed them with $ApoE^{-/-}$ mice. We also studied $ApoE^{-/-}$ mice deficient in OGG1 ($OGG1^{-/-}$). $OGG1^{-/-}$ mice showed increased 8oxoG *in vivo* and increased atherosclerosis, whereas mice expressing VSMC-specific OGG1, but not the acetylation mutant $OGG1^{K-R}$, showed markedly reduced intracellular 8oxoG and reduced atherosclerosis. VSMC OGG1 reduced telomere 8oxoG accumulation, DNA strand breaks, cell death and senescence after oxidant stress, and activation of pro-inflammatory pathways.

***Conclusions*—**We identify defective 8oxoG BER in human atherosclerotic plaque VSMCs, OGG1 as a major 8oxoG repair enzyme in VSMCs, and p300/SIRT1 as major regulators of OGG1 through acetylation/deacetylation. Reducing oxidative damage by rescuing OGG1 activity reduces plaque development, indicating the detrimental effects of 8oxoG on VSMC function.

Key Words: Atherosclerosis; DNA damage; Oxidative damage; DNA glycosylases; Vascular Disease

Clinical Perspective

What is new?

- We demonstrate that human atherosclerosis exhibits increased oxidative DNA damage and defective repair of that damage in vascular smooth muscle cells (VSMCs).
- Defective base-excision repair (BER) is due to reduced expression, acetylation and activity of the enzyme OGG1 in atherosclerosis.
- OGG1 is a major BER enzyme in VSMCs, whose activity and protein stability are regulated by acetylation through the p300acetyltransferase and sirtuin 1 deacetylase enzymes.
- Correcting the BER defect in VSMCs alone markedly reduces plaque formation, indicating that endogenous levels of oxidative DNA damage in VSMCs promote plaque development.

What are the clinical implications?

- Oxidative DNA damage accumulates slowly in atherosclerosis and disappears only very slowly when hyperlipidemia is corrected.
- Oxidative DNA damage causes inflammation, cell death and cell senescence, all of which promote atherogenesis.
- OGG1 protects VSMCs against oxidative DNA damage, identifying BER as a possible therapeutic target in atherosclerosis.
- Protection against oxidative DNA damage or increased DNA repair are beneficial over and above the standard clinical approach of reducing risk factors for coronary artery disease that promote damage, including hypercholesterolemia, diabetes mellitus, and smoking.

Non-standard Abbreviations and Acronyms

Ac-OGG1	acetyl-OGG1
ApoE	**apolipoprotein E**
BER	base excision repair
BSA	bovine serum albumin
CCL2	C-C Motif chemokine ligand 2
ChIP	chromatin immunoprecipitation
DDR	DNA damage response
GFP	green fluorescent protein
IL	interleukin
Lys	lysine
MCP1	monocyte chemotactic protein 1
NLRP	NACHT, LRR and PYD domains-containing protein
OGG1	8-oxoguanine DNA Glycosylase
PCR	polymerase chain reaction
PLA	proximity ligation assay
ROS	reactive oxygen species
SIRT1	sirtuin 1
αSMA	α-smooth muscle actin
TNFα	tumor necrosis factor α
TUNEL	terminal UTP nick end-labeling
VSMCs	vascular smooth muscle cells

Introduction

DNA bases are susceptible to oxidation mediated by reactive oxygen species (ROS). The low redox potential of guanine makes it especially vulnerable and leads to a plethora of oxidized guanine products[1]. 8-oxoguanine (8oxoG) is the most abundant DNA lesion formed upon oxidative exposure, and the presence of 8oxoG is often used as a cellular biomarker to indicate extent of oxidative stress. 8oxoG is a highly mutagenic miscoding lesion that can lead to G:C to T:A transversion mutations and is widely found in human disease and aging[2]. However, it is often unclear whether 8oxoG accumulation is just a marker of oxidative stress or has a pathogenetic role in disease.

Base excision repair (BER) is the primary mechanism for repairing 8oxoG. BER involves the concerted effort of several repair proteins that recognize and excise oxidized bases, replacing the damaged moiety with a normal nucleotide and restoring DNA integrity[3]. BER is a critical process for genomic maintenance, as highlighted by the severe phenotypes of mice deficient in BER function, including premature aging and metabolic defects[4]. However, with the exception of specific BER gene mutations, evidence of defective BER and whether it contributes to human disease is limited.

Advanced atherosclerotic plaques are characterised by 8oxoG accumulation in vascular smooth muscle cells (VSMCs), macrophages and endothelial cells[5,6]. 8oxoG also accumulates in plaques in fat-fed animals, but normalizes only slowly on a normal diet[5]. The persistence of DNA damage can reflect both ongoing damage-inducing stimuli, for example through ROS, and/or defects in DNA repair. A number of inherited defects that impair DNA repair are associated with human atherosclerosis or can promote atherosclerosis in animal models (reviewed in [7]). In contrast, whether the far lower endogenous levels of 8oxoG found in

atherosclerosis affect plaque development is not known. A recent study has showed that knockout of the DNA glycosylase 8-Oxoguanine DNA Glycosylase (OGG1) in macrophages promotes atherosclerosis, and OGG1 transcript expression was reduced in human plaques compared to normal vessels[8]; however, whether the observed decreased OGG1 expression translates into DNA repair defects is unknown.

We show that human atherosclerotic plaque VSMCs have defective 8oxoG BER, associated with decreased expression and acetylation of OGG1. We establish OGG1 as a major 8oxoG repair enzyme in VSMCs, and that OGG1 activity in VSMCs is controlled by Lys338/Lys341 acetylation. We identify p300 and sirtuin 1 (SIRT1) as major acetyltransferase and deacetylase enzymes directly targeting OGG1, and thus regulating 8oxoG BER and 8oxoG content in VSMCs. p300 expression is reduced in plaque VSMCs and by oxidative stress, and reduced formation of the p300-OGG1 complex compromises OGG1 activity and protein stability. Importantly, inhibiting endogenous oxidative damage by rescuing VSMC OGG1 markedly reduces atherosclerosis *in vivo*, an effect that requires OGG1 acetylation. Our findings indicate that human atherosclerosis is characterized by defective 8oxoG BER, and endogenous levels of oxidative DNA damage in VSMCs promote atherosclerosis.

Methods

The data that support the findings of this study are available within the article, data supplement and from the corresponding author upon reasonable request.

Human atherosclerotic plaque and normal vessels

Human tissue was obtained under informed consent using protocols approved by the Cambridge or Huntingdon Research Ethical Committee. Atherosclerotic plaques and normal aorta were

obtained from separate patients undergoing carotid endarterectomy or aortic valve replacement respectively.

Experimental animals

All *in vivo* experiments followed United Kingdom Home Office licensing and were approved by the local animal ethical committee. Transgenic mice were generated as described in the **online-only Data Supplement**. The global $OGG^{-/-}$ and SM22α-$SIRT1^{ex4/ex4}$ conditional transgenic mouse models were generated as described previously[9,10]. $OGG1^{-/-}$ mouse embryos were a gift from Christi Walter (University of Texas Health Science Center, Texas, USA).

Atherosclerosis protocols

Male and female littermate Control $ApoE^{-/-}$, SM22α-OGG1/$ApoE^{-/-}$, and SM22α-$OGG1^{K-R}$/$ApoE^{-/-}$ mice were fed High Fat 'Western' Diet (829-100, Special Diet Services, HFD-21% total fat, 0.2% cholesterol, 0% sodium cholate) from 8-22 weeks.

Histological Analysis and Oil Red O staining of descending aorta

Atherosclerosis extent and composition was analyzed as described previously[10] and in the **online-only Data Supplement**.

Cell culture

Human, rat and mouse VSMCs were cultured as described previously[11] and in the **online-only Data Supplement**.

Transfections and virus infections

Transfections and retrovirus infections were performed as described previously[10] and in the **online-only Data Supplement**.

CRISPR-mediated gene silencing

Gene silencing experiments were performed as described in the **online-only Data Supplement**.

Real-time polymerase chain reaction

Oligonucleotide sequences used are listed in **Table 1** in the **online-only Data Supplement**.

Oligonucleotide incision assay

8oxoG BER activity in nuclear lysates was determined as described previously[12] and in the **online-only Data Supplement.**

8oxoG ELISA

8oxoG levels were assessed using an ELISA assay (Abcam) as described in the **online-only Data Supplement**.

Intracellular ROS measurement

Intracellular ROS was measured as described previously[13] and in the **online-only Data Supplement**.

Annexin V/PI flow cytometry

Cell death was determined using an Apoptosis Detection kit (BD BioSciences) as described in the **online-only Data Supplement**.

Comet assay

Comet assay was performed using mouse VSMCs as described previously[11] and in the **online-only Data Supplement**.

Immunofluorescence

Immunofluorescence analysis was performed as described previously[14] and in the **online-only Data Supplement**.

Immunoprecipitation and Western blotting

Immunoprecipitation assays and Western blotting were performed as described previously[11] and in the **online-only Data Supplement**.

ChIP-qPCR

Chromatin immunoprecipitation (ChIP) was performed as described in the **online-only Data Supplement**.

Statistical analysis

Sample sizes were selected on the basis of previous experiments that identified significant differences in plaque development in mice. No randomization was applied as all mice used were genetically defined, inbred mice. Blinding was employed and no animals were excluded from analysis. Data shown are mean±SEM. Normality of distribution was determined using D'Agostino-Pearson omnibus normality tests. Statistical significance was determined by one-way analysis of variance (ANOVA) followed by Bonferroni post-test when more than two groups were compared and a two tailed Student's t-test to compare two groups of data using Prism 6.0 (Graph Pad). Differences were considered statistically significant with a P value<0.05.

Results

Human atherosclerotic plaque VSMCs show reduced BER activity

Previous studies have shown that advanced human atherosclerotic plaques display increased 8oxoG lesions in cells expressing VSMC or macrophage markers compared with normal arteries[15]. Studies also show that plaques have increased ROS content compared with normal vessels[16,17], so that increased 8oxoG may be due to increased oxidative stress within the plaque, or defective BER, or both. We therefore examined 8oxoG repair in VSMCs cultured from human carotid plaques or normal aorta from patients matched for age and sex, with cultures matched for passage number. Cells were fractionated into nuclear and cytoplasmic compartments to assay nuclear or mitochondrial BER respectively **(Supplemental Figure I)**, and 8oxoG repair activity

examined using a fluorescently-labeled 8oxoG-containing molecular beacon that can be incised and assayed in real time. Plaque VSMCs showed marked reduction in nuclear 8oxoG repair activity compared with aortic VSMCs, but cytoplasmic 8oxoG repair activity was similar in both cell types **(Figure 1a)**.

Although 8oxoG repair is mediated by a number of enzymes, knockout studies suggest that OGG1 is a major, non-redundant enzyme responsible for repairing 8oxoG from the bulk of the genome in many tissues[18] and that activation of alternate pathways cannot compensate for OGG1 deficiency. OGG1 mRNA was increased in human plaque VSMCs 1.5-fold on qPCR **(Figure 1b)**, but plaque VSMCs showed reduced total OGG1 protein expression compared to aortic VSMCs, and a marked reduction in Acetyl-OGG1 (Ac-OGG1) expression **(Figure 1c)**. To determine whether protein expression *in vitro* reflects expression in VSMCs *in vivo*, we examined 8oxoG, Ac-OGG1 and OGG1 expression in human coronary plaques from American Heart Association grade IV lesions compared with normal undiseased aorta, co-labeled with αSMA to identify VSMCs. 8oxoG lesions were increased in human plaque VSMCs **(Figure 1d).** Consistent with the *in vitro* data, human plaque VSMCs showed reduced percentage of VSMCs expressing total OGG1 and a markedly reduced percentage of VSMCs expressing Ac-OGG1 vs. aortic VSMCs **(Figure 1d)**, suggesting that increased oxidative damage in plaque VSMCs may be due to decreased expression and acetylation of OGG1.

OGG1 is a major BER enzyme in VSMCs

To determine whether OGG1 is an important regulator of 8oxoG BER in VSMCs, we knocked down OGG1 *in vitro* using CRISPR/Cas9 to delete exon 1 or 7 in rat VSMCs. OGG1 expression was efficiently and stably reduced in $OGG1^{Exon1KO}$ or $OGG1^{Exon7KO}$ cells **(Figure 2a)**, with no compensatory effect on expression of other BER enzymes such as NEIL1 and NTH

(Supplemental Figure IIa). Oxidative DNA damage was stimulated by treatment with tert-butyl hydroperoxide (t-BHP) for 1h, which induces oxidative stress and 8oxoG in VSMCs[15], cells were left to recover for 0-24h, and 8oxoG BER activity examined. t-BHP transiently inhibited BER activity in control cells which then normalized by 24h; OGG1 knockdown reduced both basal and t-BHP-induced 8oxoG BER activity, such that OGG1 was responsible for >95% of 8oxoG BER activity **(Figure 2b)**. Consistent with t-BHP-induced inhibition of BER, t-BHP also increased intracellular 8oxoG content in VSMCs **(Figure 2c)**, with recovery albeit incomplete by 24h. OGG1^{Exon1KO} and OGG1^{Exon7KO} cells showed higher basal and t-BHP-induced intracellular 8oxoG, which was completely unchanged to 24h **(Figure 2c)**, confirming that OGG1 is a major BER enzyme repairing 8oxoG in VSMCs.

Repair of 8oxoG requires OGG1 acetylation

To determine whether 8oxoG repair activity requires OGG1 acetylation in VSMCs, we stably expressed wild type human OGG1, OGG1^{K-R} or the empty vector in rat VSMCs by retrovirus-mediated gene transfer. OGG1^{K-R} is an acetylation site mutant in which Lys-338 and Lys-341 (which are active in 8oxoG repair[19]) are replaced by arginines. Exogenous human OGG1 was expressed at comparable levels in OGG1 and OGG1^{K-R} cells **(Figure 2d)**, localized to the nucleus **(Supplemental Figure IIb)**, and did not suppress endogenous rat OGG1 expression **(Figure 2d).** However, Ac-OGG1 expression was increased in OGG1 but not OGG1^{K-R} VSMCs **(Figure 2d)**. OGG1, but not OGG1^{K-R} cells showed significantly increased 8oxoG BER after t-BHP compared with control cells (Ctrl) expressing the empty vector alone **(Figure 2e)**. Ctrl, OGG1, and OGG1^{K-R} VSMCs showed similar intracellular baseline 8oxoG, and similar 8oxoG levels after 1h t-BHP treatment; however, OGG1 but not OGG1^{K-R} VSMCs displayed more rapid removal of 8oxoG **(Figure 2f)**. To exclude the possibility that expression of OGG1 altered ROS

generation by t-BHP, we examined ROS levels at baseline and after t-BHP in the 3 cell lines; ROS levels were identical in Ctrl, OGG1 and OGG1^{K-R} VSMCs at both baseline and after t-BHP **(Supplemental Figure IIc)**, indicating that OGG1 acetylation regulates efficiency of 8oxoG removal after oxidative stress without affecting ROS.

OGG1 acetylation and stability is regulated by p300

Although the acetyltransferase p300 can acetylate OGG1 in cancer cells[19], the major acetyltransferase and deacetylase enzymes of OGG1 in VSMCs are not known, or their expression in atherosclerosis. We examined p300 expression in cultured normal aortic and plaque VSMCs, and whether VSMC OGG1 and 8oxoG repair activity were regulated by p300. Both p300 mRNA (**Supplemental Figure IIIa)** and protein expression **(Figure 3a)** were reduced in plaque compared with aortic VSMCs, and the % of VSMCs expressing p300 was also reduced in plaque VSMCs *in vivo* **(Supplemental Figure IIIb)**. To examine whether oxidative stress could be the underlying cause of reduced p300 levels in plaque VSMCs, we treated control VSMCs with 1h t-BHP and examined OGG1, Ac-OGG1, and p300 protein expression up to 24h recovery. t-BHP reduced both Ac-OGG1 and p300 expression in parallel, which did not normalize by 24h **(Figure 3b, Supplemental Figure IIIc)**, suggesting that ROS-induced reduction of OGG1 acetylation is due to ROS-induced decrease in p300 expression. The reduced OGG1 acetylation and p300 expression even at 24 h after t-BHP treatment **(Figure 3b)** may explain the incomplete 8oxoG repair seen in control cells **(Figure 2c)**.

To examine whether p300 interacts with OGG1 at endogenous levels of expression in VSMCs, human VSMC lysates were immunoprecipated with an anti-p300 antibody and probed for OGG1. p300 associated with OGG1 at endogenous levels of expression, and p300 complex formation with OGG1 was reduced by t-BHP **(Figure 3c)**. Proximity ligation assay (PLA)

confirmed the p300/OGG1 interaction in human VSMCs and localized it primarily to the nucleus **(Figure 3d,** negative controls shown in **Supplemental Figure IIId)**. To determine if p300 regulates OGG1 acetylation and BER, we examined Ac-OGG1 expression and BER activity in OGG1 or OGG1^{K-R} cells treated with 1h t-BHP and 24h recovery ± CTPB, a specific activator of p300 HAT activity[20,21]. CTPB induced hyperacetylation of histone 4 as expected[22] **(Figure 3e)**. Importantly, CTPB induced acetylation of endogenous rat and exogenous human OGG1 in OGG1 cells, but human OGG1 remained unchanged in OGG1^{K-R} cells **(Figure 3e)**. CTPB also increased 8oxoG repair activity in OGG1 cells but not in OGG1^{K-R} cells **(Figure 3f, Supplemental Figure IVa)**, in line with the effects on OGG1 acetylation. Furthermore, the p300 inhibitor C646[23] inhibited BER in VSMCs (**Supplemental Figure IVb).**

Our findings that OGG1 mRNA is increased in human plaque VSMCs, but expression of OGG1 and acetylated OGG1 protein are reduced, suggests that both expression and activity of OGG1 are controlled by post-translational mechanisms. We therefore examined the stability of OGG1 protein in cells treated with cycloheximide to prevent *de novo* protein synthesis. Cycloheximide reduced expression of endogenous rat OGG1 in Ctrl, OGG1 and OGG1^{K-R} VSMCs to a similar extent; in contrast, the reduction in human OGG1 was slower in OGG1 cells compared to OGG1^{K-R} VSMCs, suggesting that acetylation of OGG1 promotes its stability **(Supplemental Figure IVc)**. To determine whether p300 regulates OGG1 stability, we repeated this experiment ± the p300 activator CTPB. CTPB enhanced the stability of OGG1 in OGG1 cells, but not in OGG1^{K-R} cells **(Figure 3g, Supplemental Figure IVd)**. We also tested whether p300 regulates OGG1 stability through its degradation. OGG1 stability was reduced in the presence of the p300 inhibitor C646, but OGG1 expression was restored after additional administration of the proteasomal inhibitor MG132 **(Figure 3h, Supplemental Figure IVe)**,

indicating that p300 regulates OGG1 expression and proteasomal-mediated degradation through its acetylation.

SIRT1 is an OGG1 deacetylase in VSMCs

The deacetylase responsible for inhibiting OGG1 activity in VSMCs is unknown, as although OGG1 interacts with class I histone deacetylases, previous studies showed that activity was not affected by the SIRT1 inhibitor nicotinamide[19]. We therefore examined whether VSMC OGG1 and BER activity were regulated by SIRT1.

To determine whether OGG1 interacts with and is deacetylated by SIRT1, we generated VSMCs that stably express wild type human SIRT1 or the deacetylase-deficient mutant $SIRT1^{H365Y}$ by retrovirus-mediated gene transfer[10]. VSMCs expressing the empty vector (Ctrl), SIRT1 or $SIRT1^{H-Y}$ were treated with t-BHP and SIRT1, Ac-OGG1 and OGG1 protein expression examined. SIRT1 but not $SIRT1^{H-Y}$ reduced Ac-OGG1 and total OGG1 expression **(Figure 4a)**, suggesting that OGG1 is a SIRT1 deacetylation substrate. Indeed, SIRT1 co-immunoprecipitated with OGG1 both at endogenous levels and when overexpressed **(Figure 4b)**, and PLA in human VSMCs confirmed this protein interaction at endogenous levels **(Figure 4c, Supplemental Figure Va)**. Consistent with SIRT1 reducing OGG1 acetylation, SIRT1 but not $SIRT1^{H-Y}$ reduced 8oxoG repair activity **(Figure 4d, Supplemental Figure Vb)**, and increased intracellular 8oxoG content **(Figure 4e)**. SIRT1 but not $SIRT1^{H-Y}$ also reduced OGG1 stability **(Figure 4f)**, consistent with SIRT1 deacetylation of OGG1. Since SIRT1 is both regulated by redox-mediated mechanisms and can inhibit ROS generation (reviewed in [24,25]), the differences in 8oxoG levels after t-BHP could be due to different levels of ROS induced in each cell type; however, ROS levels in Ctrl, SIRT1 or $SIRT1^{H-Y}$ cells after t-BHP were similar **(Supplemental Figure Vc)**. Finally, we examined expression of OGG1 and Ac-OGG1 in aortas from $ApoE^{-/-}$

mice that express a truncated inactive SIRT1 (SIRT1$^{\Delta ex4/\Delta ex4}$) from the SMC-specific SM22α (transgelin, *Tagln*) promoter[10]. SIRT1 expression was detectable in <1% of VSMCs in SM22-SIRT1$^{\Delta ex4/\Delta ex4}$ ApoE$^{-/-}$ mice, confirming the efficacy of the recombination. OGG1 expression was seen at similar levels in SM22-SIRT1$^{\Delta ex4/\Delta ex4}$ ApoE$^{-/-}$ and control mice; in contrast Ac-OGG1 expression was increased in SM22-SIRT1$^{\Delta ex4/\Delta ex4}$ ApoE$^{-/-}$ mice consistent with SIRT1 deacetylation of OGG1 **(Figure 4g)**. Together these data indicate that SIRT1 binds to and regulates OGG1deacetylation and stability, and thus regulates oxidative damage in VSMCs.

VSMC OGG1 reduces oxidative damage and atherosclerosis in vivo

Whole body or bone marrow cell-restricted knockout of OGG1 results in increased atherosclerosis in low density lipoprotein receptor-null mice[8]. However, OGG1 knockout results in massive 8oxoG accumulation, and the effects of endogenous levels of 8oxoG found in atherosclerosis and VSMC OGG1 are not known. We therefore generated mice expressing myc-tagged human OGG1 or OGG1^{K-R} from the minimal SM22α promoter (SM22α-OGG1 or SM22α-OGG1^{K-R} mice). This promoter is expressed in VSMCs in large arteries only[26], and has an additional deletion of the CARG motif to prevent promoter down-regulation during VSMC phenotypic change in atherosclerosis[27]. SM22α-OGG1 and SM22α-OGG1^{K-R} mice were compared against control mice and OGG1$^{-/-}$ mice[9]. Mouse OGG1 mRNA expression was markedly reduced in all tissues in OGG1$^{-/-}$ mice, but not affected by co-expression of human OGG1 in SM22α-OGG1 or SM22α-OGG1^{K-R} mice **(Supplemental Figure VIa)**. Previous studies have also shown that the full-length SM22α promoter is also expressed in myeloid cells[28]; in contrast, the minimal SM22α promoter-driven human OGG1 transgene was only expressed in aortas of SM22α-OGG1 mice, but not peripheral blood, bone marrow cells or spleen **(Supplemental Figure VIb)**.

OGG1 protein expression was markedly reduced in VSMCs cultured from OGG1$^{-/-}$ mice, but increased in SM22α-OGG1 and SM22α-OGG1^{K-R} mice to similar levels (**Figure 5a)**. Ac-OGG1 expression was increased in SM22α-OGG1 mouse VSMCs but not SM22α-OGG1^{K-R} VSMCs, while myc tag expression was observed only in transgenic lines (**Figure 5a)**. ELISA of cultured VSMCs from these mice showed increased 8oxoG in OGG1$^{-/-}$ mice, and reduced 8oxoG in SM22α-OGG1 but not SM22 α-OGG1^{K-R} mice **(Figure 5b)**. 8oxoG repair activity was increased in SM22α-OGG1 VSMCs, reduced in OGG1$^{-/-}$ VSMCs, but unchanged in SM22α-OGG1^{K-R} VSMCs compared with control cells **(Figure 5c, Supplemental Figure Vic)**. Thus, OGG1$^{-/-}$ mice allow examination of the effect of supraphysiological levels of 8oxoG in all tissues on atherosclerosis; SM22α-OGG1 mice allow determination of the effect of rescuing OGG1 activity and suppressing endogenous levels of 8oxoG in VSMCs only, and SM22α-OGG1^{K-R} mice provide the acetylation-mutant control for SM22α-OGG1 mice.

Control wild type, OGG1$^{-/-}$, SM22α-OGG1 and SM22α-OGG1^{K-R} mice were crossed onto an ApoE$^{-/-}$ background, weaned at 6 weeks and male and female littermates were fat fed from 8-22 weeks of age. Weight gain **(Supplemental Figure VIIa)**, serum lipids (**Supplemental Figure VIIb),** systolic, diastolic and mean arterial pressures, and heart rates were similar across all groups pre- and post- fat feeding **(Supplemental Figure VIIc)**. Atherosclerosis was increased in the descending aorta and aortic root in OGG1$^{-/-}$ ApoE$^{-/-}$ mice compared with controls **(Figure 6a, 6b)**, but markedly decreased in both vascular beds in SM22α-OGG1 ApoE$^{-/-}$ mice; this protective effect was lost in SM22α-OGG1^{K-R} ApoE$^{-/-}$ mice. Both necrotic core and fibrous cap areas were reduced in SM22α-OGG1 ApoE$^{-/-}$ mice **(Figure 6c)** compared to controls, with no overall change in relative proportions of the necrotic core and fibrous cap to the plaque or to each other **(Supplemental Figure VIIIa)**. Analyses of male and female mice were grouped

together **(Supplemental Figure VIIIb)** as we found no significant differences between sexes for any parameters measured except for body weight (not shown). Aortic plaques in SM22α-OGG1 mice had reduced 8oxoG levels compared to SM22α-OGG1^{K-R} and control mice, correlating with reduced plaque area, and significantly fewer TUNEL-positive apoptotic cells compared to SM22α-OGG1^{K-R} mice **(Supplemental Figure VIIIc)**.

Oxidative DNA damage accumulates at telomeres, and induces strand breaks, cell senescence, apoptosis, and drives inflammation

Although VSMC OGG1 protected against atherosclerosis, the underlying mechanisms, which may be multiple, are unclear. For example, defects in BER can cause DNA strand breaks resulting in cell death. Indeed, OGG1$^{-/-}$ VSMCs showed increased DNA strand breaks after t-BHP treatment with a reduced rate of repair; DNA damage was lower in SM22α- OGG1 but not SM22α-OGG1^{K-R} VSMCs vs. control cells **(Figure 7a)**. 8oxoG accumulation at telomeres can result in cell senescence and subsequent inflammation. Indeed ChIP-qPCR showed that OGG1$^{-/-}$ VSMCs had increased 8oxoG accumulation at telomeres, and this was reduced in SM22α-OGG1, but not SM22α-OGG1^{K-R} cells **(Figure 7b)**. The % of cells expressing senescence-associated β-galactosidase after t-BHP was increased in OGG1$^{-/-}$ VSMCs, but reduced in SM22α-OGG1, but not SM22α- OGG1^{K-R} cells **(Figure 7c, Supplemental Figure IX)**. Finally, t-BHP-induced cell death was increased in OGG1$^{-/-}$, and reduced in SM22α-OGG1 but not SM22α- OGG1^{K-R} cells **(Figure 7d)**, indicating that OGG1 overexpression protects VSMCs against apoptosis, but this depends upon OGG1 acetylation**.**

Oxidized DNA can also activate the inflammasome, resulting in release of pro-inflammatory cytokines such as IL-1β[8]. Using qPCR, we profiled aortic arch tissue from ApoE$^{-/-}$ mice after high fat diet feeding for levels of inflammatory cytokines and inflammasome

components. SM22α-OGG1 ApoE$^{-/-}$ aortic tissue contained significantly decreased levels of transcripts for cytokines IL1β, IL6, CCL2/MCP1 and TNFα and inflammasome components NLRP1 and NLRP3 **Figure 7e**, indicative of a shift toward a more anti-inflammatory phenotype, with an opposite profile seen in OGG1$^{-/-}$ ApoE$^{-/-}$ mice. Serum levels of IL1β, IL6, CCL2/MCP1 and TNFα were also decreased in SM22α-OGG1 ApoE$^{-/-}$ mice after high fat diet feeding compared to controls (**Supplemental Figure Xa)**. To identify the source of these cytokines, we cultured VSMCs from these mice and determined cytokine secretion following t-BHP treatment for 24h. t-BHP did not increase levels of IL1β, IL6, MCP1 and TNFα in conditioned media of SM22α-OGG1 ApoE$^{-/-}$ cells, compared to SM22α-OGG1$^{K\text{-}R}$ ApoE$^{-/-}$ and control ApoE$^{-/-}$ cells (**Supplemental Figure Xb**). The anti-inflammatory profile *in vivo* of OGG1 mice and in culture of OGG1 VSMCs suggests that 8oxoG in VSMCs may exert a direct pro-inflammatory effect on the vessel wall.

Discussion

Advanced human atherosclerotic plaques demonstrate extensive 8oxoG accumulation in multiple cell types[5,6], and polymorphisms in some BER enzymes are associated with myocardial infarction[29], suggesting that impaired BER might promote plaque development or instability. Indeed, OGG1 knockout in hematopoietic cells promotes atherogenesis and enhanced inflammasome activation in macrophages[8]. However, VSMCs are long–lived cells[30], and the effects of oxidative DNA damage in VSMCs in atherosclerosis are not known. In particular, chronic oxidative stress can increase 8oxoG levels >250-fold without apparent severe consequences[31], and OGG1$^{-/-}$ mice are born and develop normally with a normal lifespan, despite a 7-fold increase 8oxoG in nuclear DNA and a >20-fold increase in mitochondrial DNA[9,32-34].

More controversially, some studies suggest that 8oxoG may actually protect against inflammation-induced DNA damage[35-37].

Our study reports a number of novel findings. In particular, we demonstrate **(a)** evidence of defective 8oxoG BER in human plaque VSMCs, not just increased damage or reduced expression of BER enzymes, **(b)** reducing physiological 8oxoG levels reduces atherosclerosis, in addition to the detrimental effects of artificially-elevated 8oxoG, **(c)** the importance of OGG1 acetylation to its function *in vivo*, **(d)** that SIRT1 regulates OGG1 acetylation *in vivo*, and **(e)** that p300 regulates OGG1 stability, not just activity. Specifically, we find that OGG1 is a major BER enzyme in VSMCs, whose activity and protein stability are regulated by acetylation. Nuclear 8oxoG repair is defective in human atherosclerotic plaque VSMCs, associated with reduced acetylation of OGG1, which results in proteasomal-mediated OGG1 degradation and reduced activity. Our findings identify that atherosclerosis is a disease characterised by defective BER in VSMCs, and that endogenous levels of oxidative DNA damage in VSMCs promote plaque development.

Human atherosclerotic plaques show a variety of DNA damage, including single and double strand breaks, telomere shortening, oxidative DNA damage and mutations (reviewed in [7]). Plaque VSMCs also show differences in expression of multiple DNA damage repair (DDR) proteins, indicative of activation of a DDR response[11]. Some human DNA damage syndromes are associated with premature atherosclerosis, and previous studies in mice have shown that knockout of some DNA repair enzymes can promote atherosclerosis or vascular dysfunction[8,38], suggesting that DNA damage may promote atherosclerosis. Indeed, a recent study showed downregulation of OGG1 transcripts in human plaque tissue compared with normal vessels[8]. In contrast, we find that OGG1 mRNA is increased in human plaque VSMCs, while total OGG1

protein expression is decreased compared to aortic VSMCs. This difference is likely due to the analyses being performed in whole plaque tissue[8], which contains a heterogeneous mixture of cells, versus VSMC cultures in this study. However, this is the first study to demonstrate that human atherosclerosis exhibits a DNA repair defect in VSMCs, that defect is due to reduced expression, acetylation and activity of a specific DNA repair protein, and that correction of that defect in VSMCs alone can markedly reduce plaque formation.

Vascular smooth muscle cells in the normal vessel wall are characterized by low rates of cell division, cell death, and cell senescence, and maintain a contractile phenotype that expresses low levels of inflammatory cytokines (reviewed in [39]). In contrast, VSMCs in atherosclerotic plaques or cultured from plaques show higher rates of cell death and cell senescence, accompanied by secretion of a variety of pro-inflammatory cytokines, some of which may be due to cell senescence[40,41]. Cell death and cell senescence promote both plaque development and plaque progression in atherosclerosis[42,43]. Oxidative DNA damage may affect multiple processes within VSMCs, and we show that VSMCs lacking OGG1 show increased cell death, cell senescence and expression of inflammasome components, all of which are pro-atherogenic, and all of which can be inhibited by overexpression of OGG1 after oxidative stress. Loss of OGG1 also increases oxidized mitochondrial DNA, inflammasome activation, and apoptosis in macrophages[8]. However, the profound reduction in plaque formation in SM22α-OGG1 compared with control mice demonstrates that endogenous levels of 8oxoG found in VSMCs in atherosclerosis promote plaque development, and emphasize the importance of oxidative DNA damage-mediated activation of cell death and senescence in VSMCs, and of VSMC-driven inflammation in atherogenesis.

Our data also demonstrate the complex effects of oxidative stress in DNA repair. Acetylation regulates multiple protein properties, such as stability, localization, function and protein-protein interactions[44]. OGG1-mediated BER activity is regulated by acetylation of lysines K338/K341 ([19] and shown here). Previous work in mouse embryonic fibroblasts showed decreased OGG1$^{K\text{-}R}$ repair activity *in vitro*[19], but not the total loss of activity we observe in VSMCs, implying that acetylation may be a more important modification for OGG1 activity in VSMCs compared with other cell types. We also show that p300 and SIRT1 are major acetyltransferase and deacetylase enzymes respectively for OGG1 acetylation, but the mechanisms of their effects, and the effects of oxidative stress may differ between cells. For example, although p300 can interact with OGG1 in some cell types[19], oxidative stress enhances histone acetyltransferase activity of p300 in lung cells with no change in expression; in contrast, p300 protein expression was downregulated following oxidative stress in VSMCs. Consistent with previous studies[19] ROS also transiently decreased OGG1 activity directly, which may be due to the reduced state of the redox-sensitive residues that determine its glycosylase activity[45,46]. Our findings emphasise the detrimental effect of chronic oxidative stress in atherosclerosis through a positive feedback loop to generate further oxidative DNA damage. ROS induce oxidative DNA damage but also impair 8oxoG BER by downregulating OGG1 directly, and indirectly through inhibiting p300 expression and thus OGG1 acetylation and protein stability. This finding may explain the observation that oxidative DNA damage persists much longer in atherosclerosis than other forms of DNA damage, even when the pro-atherogenic stimulus is removed[5].

Although the regulation of OGG1 activity by acetylation is known[19], the identity of the OGG1 deacetylase has not been proven. SIRT1 is a NAD^+-dependent lysine deacetylase with

roles including cell ageing, genomic stability and cell apoptosis[47], but it has been excluded previously as the SIRT1 inhibitor nicotinamide did not increase OGG1 acetylation in HCT116 cells[19]. However, an association of SIRT1 and OGG1 was not tested directly, and we have found that SIRT1 substrates are tissue-specific[10]. We identify that SIRT1 is a major enzyme regulating OGG1 activity, and its activity depends upon its ability to deacetylate OGG1. Thus, SIRT1 but not SIRT1^{HY} reduces OGG1 acetylation, reduces 8oxoG repair and promotes persistence of oxidative DNA damage. SIRT1 deletion *in vivo* also increases Ac-OGG1, indicating that SIRT1 can regulate OGG1 activity at endogenous levels. However, SIRT1 is downregulated in human atherosclerotic plaques, and in plaque and senescent VSMCs compared with normal VSMCs in culture[10], suggesting that SIRT1 regulation of OGG1 may be particularly relevant in normal arteries as a way of deactivating OGG1 when oxidative DNA repair is complete, but less important in atherosclerosis where the reduced p300 expression results in reduced acetylated OGG1. However, SIRT1 also activates other components of the BER pathway including the enzymes Thymine DNA Glycosylase, Apurinic/apyrimidinic endonuclease 1 and Poly(ADP-Ribose) Polymerase 1[48,49], which may partly explain the profound effect of VSMC SIRT1 knockout in atherosclerosis[10].

Our findings are consistent with the following model **(Figure 8)**. OGG1 is preferentially acetylated by p300 in acute oxidative stress conditions that require 8oxoG repair activity, leading to efficient 8oxoG BER. Ac-OGG1 is deacetylated by SIRT1 when 8oxoG BER is complete. However, chronic oxidative stress in atherosclerosis results in downregulation of p300 and p300-mediated acetylation of OGG1, which in turn reduces OGG1 protein stability and thus expression, and overall 8oxoG repair activity. ROS may also reduce OGG1 activity directly via its effects on redox-sensitive residues and glycosylase activity[45,46]. 8oxoG accumulation in

VSMCs results in DNA strand breaks, cell senescence, cell death, inflammasome activation and increased secretion of pro-inflammatory cytokines, all of which promote atherogenesis. Rescue of VSMC OGG1 prevents 8oxoG accumulation and these consequences, protecting against atherosclerosis.

In summary, we have identified that 8oxoG repair is reduced in VSMCs in human atherosclerosis, due to chronic oxidative stress-induced reduction in expression, stability, acetylation and activity of OGG1. SIRT1 is also a major regulator of OGG1 acetylation, expression and activity. OGG1 protects VSMCs against oxidative DNA damage, cell senescence and apoptosis, and reduces atherosclerosis formation, identifying BER as a possible therapeutic target in atherosclerosis.

Sources of Funding

This work was funded by grants from the British Heart Foundation (BHF) (RG/13/14/30314 and PG/11/112/29272, the Oxbridge BHF Centre for Regenerative Medicine (RM/13/3/30159), the BHF Centre for Cardiovascular Research Excellence, and the National Institute for Health Research (NIHR) Cambridge Biomedical Research Centre.

Disclosures

None

References

1. Neeley WL, Essigmann JM. Mechanisms of formation, genotoxicity, and mutation of guanine oxidation products. Chem Res Toxicol. 2006;19:491-505.
2. Grollman AP, Moriya M. Mutagenesis by 8-oxoguanine: an enemy within. Trends Genet. 1993;9:246-249.

3. Hoeijmakers JH. Genome maintenance mechanisms for preventing cancer. Nature. 2001;411:366-374.
4. Vartanian V, Lowell B, Minko IG, Wood TG, Ceci JD, George S, Ballinger SW, Corless CL, McCullough AK, Lloyd RS. The metabolic syndrome resulting from a knockout of the NEIL1 DNA glycosylase. Proc Natl Acad Sci USA. 2006;103:1864-1869.
5. Martinet W, Knaapen MW, De Meyer GR, Herman AG, Kockx MM. Oxidative DNA damage and repair in experimental atherosclerosis are reversed by dietary lipid lowering. Circ Res. 2001;88:733-739.
6. Martinet W, Knaapen MW, De Meyer GR, Herman AG, Kockx MM. Elevated levels of oxidative DNA damage and DNA repair enzymes in human atherosclerotic plaques. Circulation. 2002;106:927-932.
7. Uryga A, Gray K, Bennett M. DNA Damage and Repair in Vascular Disease. Annu Rev Physiol. 2016;78:45-66.
8. Tumurkhuu G, Shimada K, Dagvadorj J, Crother TR, Zhang W, Luthringer D, Gottlieb RA, Chen S, Arditi M. Ogg1-Dependent DNA Repair Regulates NLRP3 Inflammasome and Prevents Atherosclerosis. Circ Res. 2016;119:e76-90.
9. Klungland A, Rosewell I, Hollenbach S, Larsen E, Daly G, Epe B, Seeberg E, Lindahl T, Barnes DE. Accumulation of premutagenic DNA lesions in mice defective in removal of oxidative base damage. Proc Natl Acad Sci USA. 1999;96:13300-13305.
10. Gorenne I, Kumar S, Gray K, Figg N, Yu H, Mercer J, Bennett M. Vascular smooth muscle cell sirtuin 1 protects against DNA damage and inhibits atherosclerosis. Circulation. 2013;127:386-396.
11. Gray K, Kumar S, Figg N, Harrison J, Baker L, Mercer J, Littlewood T, Bennett M. Effects of DNA damage in smooth muscle cells in atherosclerosis. Circ Res. 2015;116:816-826.
12. German P, Szaniszlo P, Hajas G, Radak Z, Bacsi A, Hazra TK, Hegde ML, Ba X, Boldogh I. Activation of cellular signaling by 8-oxoguanine DNA glycosylase-1-initiated DNA base excision repair. DNA Repair (Amst). 2013;12:856-863.
13. Mercer JR, Cheng KK, Figg N, Gorenne I, Mahmoudi M, Griffin J, Vidal-Puig A, Logan A, Murphy MP, Bennett M. DNA damage links mitochondrial dysfunction to atherosclerosis and the metabolic syndrome. Circ Res. 2010;107:1021-1031.
14. Mahmoudi M, Gorenne I, Mercer J, Figg N, Littlewood T, Bennett M. Statins use a novel Nijmegen breakage syndrome-1-dependent pathway to accelerate DNA repair in vascular smooth muscle cells. Circ Res. 2008;103:717-725.
15. Matthews C, Gorenne I, Scott S, Figg N, Kirkpatrick P, Ritchie A, Goddard M, Bennett M. Vascular smooth muscle cells undergo telomere-based senescence in human atherosclerosis: effects of telomerase and oxidative stress. Circ Res. 2006;99:156-164.
16. Warnholtz A, Nickenig G, Schulz E, Macharzina R, Brasen J, Skatchov M, Heitzer T, Stasch J, Greindling K, Harrison D, Bohm M, Meinertz T, Munzel T. Increased NADH-oxidase-mediated superoxide production in the early stages of atherosclerosis.Evidence forthe involvement of the renin-angiotensin system. Circulation. 1999;99:2027-2033.
17. Hathaway CA, Heistad DD, Piegors DJ, Miller FJ, Jr. Regression of atherosclerosis in monkeys reduces vascular superoxide levels. Circ Res. 2002;90:277-283.
18. Nishimura S. Involvement of mammalian OGG1(MMH) in excision of the 8-Hydroxyguanine residue in DNA. Free Radic Biol Med. 2002;32:813-821.

19. Bhakat KK, Mokkapati SK, Boldogh I, Hazra TK, Mitra S. Acetylation of human 8-oxoguanine-DNA glycosylase by p300 and its role in 8-oxoguanine repair in vivo. Mol Cell Biol. 2006;26:1654-1665.
20. Balasubramanyam K, Swaminathan V, Ranganathan A, Kundu TK. Small molecule modulators of histone acetyltransferase p300. J Biol Chem. 2003;278:19134-19140.
21. Mantelingu K, Kishore AH, Balasubramanyam K, Kumar GV, Altaf M, Swamy SN, Selvi R, Das C, Narayana C, Rangappa KS, Kundu TK. Activation of p300 histone acetyltransferase by small molecules altering enzyme structure: probed by surface-enhanced Raman spectroscopy. J Phys Chem B. 2007;111:4527-4534.
22. Prieur A, Besnard E, Babled A, Lemaitre JM. p53 and p16(INK4A) independent induction of senescence by chromatin-dependent alteration of S-phase progression. Nat Commun. 2011;2:473. doi 10.1038/ncomms1473
23. Bowers EM, Yan G, Mukherjee C, Orry A, Wang L, Holbert MA, Crump NT, Hazzalin CA, Liszczak G, Yuan H, Larocca C, Saldanha SA, Abagyan R, Sun Y, Meyers DJ, Marmorstein R, Mahadevan LC, Alani RM, Cole PA. Virtual ligand screening of the p300/CBP histone acetyltransferase: identification of a selective small molecule inhibitor. Chem Biol. 2010;17:471-482.
24. Hwang JW, Yao H, Caito S, Sundar IK, Rahman I. Redox regulation of SIRT1 in inflammation and cellular senescence. Free Radic Biol Med. 2013;61:95-110.
25. Salminen A, Kaarniranta K, Kauppinen A. Crosstalk between Oxidative Stress and SIRT1: Impact on the Aging Process. Int J Mol Sci. 2013;14:3834-3859.
26. Li L, Miano JM, Mercer B, Olson EN. Expression of the SM22alpha promoter in transgenic mice provides evidence for distinct transcriptional regulatory programs in vascular and visceral smooth muscle cells. J Cell Biol. 1996;132:849-859.
27. Regan CP, Adam PJ, Madsen CS, Owens GK. Molecular mechanisms of decreased smooth muscle differentiation marker expression after vascular injury. J Clin Invest. 2000;106:1139-1147.
28. Shen Z, Li C, Frieler RA, Gerasimova AS, Lee SJ, Wu J, Wang MM, Lumeng CN, Brosius FC, 3rd, Duan SZ, Mortensen RM. Smooth muscle protein 22 alpha-Cre is expressed in myeloid cells in mice. Biochem Biophys Res Commun. 2012;422:639-642.
29. Skarpengland T, Laugsand LE, Janszky I, Luna L, Halvorsen B, Platou CG, Wang W, Vatten LJ, Damas JK, Aukrust P, Bjoras M, Asvold BO. Genetic variants in the DNA repair gene NEIL3 and the risk of myocardial infarction in a nested case-control study. The HUNT Study. DNA Repair (Amst). 2015;28:21-27.
30. Goncalves I, Stenstrom K, Skog G, Mattsson S, Nitulescu M, Nilsson J. Short communication: Dating components of human atherosclerotic plaques. Circ Res. 2010;106:1174-1177.
31. Arai T, Kelly VP, Minowa O, Noda T, Nishimura S. High accumulation of oxidative DNA damage, 8-hydroxyguanine, in Mmh/Ogg1 deficient mice by chronic oxidative stress. Carcinogenesis. 2002;23:2005-2010.
32. Minowa O, Arai T, Hirano M, Monden Y, Nakai S, Fukuda M, Itoh M, Takano H, Hippou Y, Aburatani H, Masumura K, Nohmi T, Nishimura S, Noda T. Mmh/Ogg1 gene inactivation results in accumulation of 8-hydroxyguanine in mice. Proc Natl Acad Sci USA. 2000;97:4156-4161.
33. de Souza-Pinto NC, Eide L, Hogue BA, Thybo T, Stevnsner T, Seeberg E, Klungland A, Bohr VA. Repair of 8-oxodeoxyguanosine lesions in mitochondrial DNA depends on the

oxoguanine DNA glycosylase (OGG1) gene and 8-oxoguanine accumulates in the mitochondrial DNA of OGG1-defective mice. Cancer Res. 2001;61:5378-5381.
34. Larsen E, Reite K, Nesse G, Gran C, Seeberg E, Klungland A. Repair and mutagenesis at oxidized DNA lesions in the developing brain of wild-type and Ogg1-/- mice. Oncogene. 2006;25:2425-2432.
35. Touati E, Michel V, Thiberge JM, Wuscher N, Huerre M, Labigne A. Chronic Helicobacter pylori infections induce gastric mutations in mice. Gastroenterology. 2003;124:1408-1419.
36. Touati E, Michel V, Thiberge JM, Ave P, Huerre M, Bourgade F, Klungland A, Labigne A. Deficiency in OGG1 protects against inflammation and mutagenic effects associated with H. pylori infection in mouse. Helicobacter. 2006;11:494-505.
37. Mabley JG, Pacher P, Deb A, Wallace R, Elder RH, Szabo C. Potential role for 8-oxoguanine DNA glycosylase in regulating inflammation. FASEB J. 2005;19:290-292.
38. Durik M, Kavousi M, van der Pluijm I, Isaacs A, Cheng C, Verdonk K, Loot AE, Oeseburg H, Bhaggoe UM, Leijten F, van Veghel R, de Vries R, Rudez G, Brandt R, Ridwan YR, van Deel ED, de Boer M, Tempel D, Fleming I, Mitchell GF, Verwoert GC, Tarasov KV, Uitterlinden AG, Hofman A, Duckers HJ, van Duijn CM, Oostra BA, Witteman JC, Duncker DJ, Danser AH, Hoeijmakers JH, Roks AJ. Nucleotide excision DNA repair is associated with age-related vascular dysfunction. Circulation. 2012;126:468-478.
39. Garrido A, Bennett M. Assessment and consequences of cell senescence in atherosclerosis. Curr Op Lipid. 2016;27:431-438.
40. Bennett M, Evan G, Schwartz S. Apoptosis of human vascular smooth muscle cells derived from normal vessels and coronary atherosclerotic plaques. J. Clin. Invest. 1995;95:2266-2274.
41. Gardner SE, Humphry M, Bennett MR, Clarke MC. Senescent vascular smooth muscle cells drive inflammation through an Interleukin-1alpha-dependent senescence-sssociated secretory phenotype. Arterioscler Thromb Vasc Biol. 2015;35:1963-1974.
42. Wang J, Uryga AK, Reinhold J, Figg N, Baker L, Finigan A, Gray K, Kumar S, Clarke M, Bennett M. Vascular smooth muscle cell senescence promotes atherosclerosis and features of plaque vulnerability. Circulation. 2015;32:1909-1919.
43. Childs BG, Baker DJ, Wijshake T, Conover CA, Campisi J, van Deursen JM. Senescent intimal foam cells are deleterious at all stages of atherosclerosis. Science. 2016;354:472-477.
44. Spange S, Wagner T, Heinzel T, Kramer OH. Acetylation of non-histone proteins modulates cellular signalling at multiple levels. Int J Biochem Cell Biol. 2009;41:185-198.
45. Jaiswal M, LaRusso NF, Nishioka N, Nakabeppu Y, Gores GJ. Human Ogg1, a protein involved in the repair of 8-oxoguanine, is inhibited by nitric oxide. Cancer Res. 2001;61:6388-6393.
46. Bravard A, Vacher M, Gouget B, Coutant A, de Boisferon FH, Marsin S, Chevillard S, Radicella JP. Redox regulation of human OGG1 activity in response to cellular oxidative stress. Mol Cell Biol. 2006;26:7430-7436.
47. Finkel T, Deng CX, Mostoslavsky R. Recent progress in the biology and physiology of sirtuins. Nature. 2009;460:587-591.

48. Madabushi A, Hwang BJ, Jin J, Lu AL. Histone deacetylase SIRT1 modulates and deacetylates DNA base excision repair enzyme thymine DNA glycosylase. Biochem J. 2013;456:89-98.
49. Yamamori T, DeRicco J, Naqvi A, Hoffman TA, Mattagajasingh I, Kasuno K, Jung SB, Kim CS, Irani K. SIRT1 deacetylates APE1 and regulates cellular base excision repair. Nucleic Acids Res. 2010;38:832-845.

Figure Legends

Figure 1. Human plaque VSMCs show defective nuclear base excision repair activity and reduced acetyl-OGG1 expression

(a) BER assay measuring incision of a fluorescently-labelled 8oxoG.C oligonucleotide in nuclear and cytoplasmic fractions of cultured plaque and normal aortic VSMCs. Representative gel (left panel) and quantification (right panel) are shown. Incision product denoted by an arrow (*n*=4). **(b)** qPCR analysis of OGG1 expression in cultured plaque and normal aortic VSMCs (*n*=4). **(c)** Western blot of OGG1 and acetylated OGG1 (Ac-OGG1) in plaque and normal aortic VSMCs (*n*=4). **(d**) Immunohistochemistry for 8oxoG, Ac-OGG1, or OGG1 (brown) in sections of human plaques and normal aorta (*n*=10). Sections are also co-stained for αSMA (blue). Insets show high power views of outlined areas. Negative controls using isotype-matched antibodies and quantification are shown below. Scale bars, 25μm. All graphical data are mean ± SEM, *P< 0.05, **P< 0.01, Student's t-test.

Figure 2. OGG1 is the major BER enzyme for 8oxoG and its activity is regulated by acetylation

(a) OGG1 protein expression in control or OGG1 exon1 or exon7 CRISPR knockout rat VSMC lines (*n*=4). **(b)** BER assay analysis and **(c)** 8oxoG intracellular levels measured by ELISA in control (Ctrl), $OGG1^{Exon1KO}$ or $OGG1^{Exon7KO}$ rat VSMCs at untreated baseline (-) or after t-BHP treatment for 1h (t=0) and after t-BHP removal (4, 8, 24h recovery) (*n*=5). **(d)** Western blot of OGG1, Ac-OGG1, or myc tag in rat VSMCs expressing the empty vector (Ctrl), human OGG1 (OGG1) or acetylation mutant OGG1 ($OGG1^{K-R}$). Immunoblotting for OGG1 shows a lower

band for endogenous rat OGG1 and a higher band for exogenous human OGG1 (*n*=4). **(e)** BER assay analysis and **(f)** 8oxoG intracellular levels measured by ELISA in Ctrl, OGG1 or OGG1^{K-R} cells at untreated baseline (-) or after t-BHP treatment for 1h (t=0) and after t-BHP removal (4, 8, 24h recovery) (*n*=4). All graphical data are mean ± SEM, *P< 0.05, **P< 0.01, ***P< 0.001, one-way ANOVA (Bonferroni post hoc).

Figure 3. p300 is downregulated in plaque VSMCs and regulates OGG1 acetylation and BER

(a) Western blot of p300 expression in cultured human plaque or normal aortic VSMCs (*n*=4). **(b)** Western blot of OGG1, Ac-OGG1 and p300 levels in human VSMCs after 1h t-BHP treatment and 0-24h recovery (*n*=4). **(c)** Immunoprecipitation of human VSMC lysates with an anti-p300 antibody analysed by immunoblotting (IB) with anti-OGG1 and anti-p300 antibodies (*n*=3). **(d)** Proximity ligation assay of OGG1-p300 interaction using rabbit anti-OGG1 and mouse anti-p300 antibodies (*n*=3). Scale bar, 20μm. **(e)** Western blot for Ac-OGG1 and Ac-Histone 4(H4) in VSMCs expressing OGG1 or OGG1^{K-R} ± CTPB treatment (10μM) (*n*=3). **(f)** Quantification of BER assay in OGG1 or OGG1^{K-R} VSMCs either untreated (-), after 1h t-BHP (0) or 6h recovery ± CTPB (*n*=3). Representative gel is shown in **Supplemental Figure IVa**. **(g)** Western blot of OGG1 expression after cycloheximide (CHX) treatment (0-4h) in OGG1 or OGG1^{K-R} VSMCs ± p300 activator CTPB (*n*=3). **(h)** Western blot of OGG1 expression after cycloheximide (CHX) treatment (0-4h) in control cells ± CTPB ± proteasomal degradation inhibitor MG132 (10 μM)(*n*=3). Scale bars, 25μm. All graphical data are mean ± SEM, *P< 0.05, Student's t-test.

Figure 4. SIRT1 binds OGG1 and regulates deacetylation of OGG1 *in vitro* and *in vivo*

(a) Western blot of total SIRT1, Ac-OGG1 and OGG1 expression in rat VSMCs expressing the empty vector (Ctrl), human SIRT1 (SIRT1) or deacetylase defective mutant $SIRT^{H364Y}$ cells after 1h t-BHP treatment and after 0-6h recovery (*n*=3). Immunoblotting for SIRT1 shows a lower band for endogenous rat SIRT1 and a higher band for exogenous human SIRT1. **(b)** Immunoprecipitation of human VSMC lysates with an anti-SIRT1 antibody analysed by immunoblotting (IB) with anti-SIRT1 and anti-OGG1 antibodies (*n*=3). **(c)** Proximity ligation assay of OGG1-SIRT1 interaction using rabbit anti-OGG1 and mouse anti-SIRT1 antibodies (*n*=3). **(d)** Quantification of BER assay in Ctrl, SIRT1 or $SIRT^{1H-Y}$ VSMCs either untreated (-), after 1h t-BHP (0) or 0-24h recovery (*n*=3). Representative gel is shown in Figure Vb in the online-only Data Supplement. **(e)** 8oxoG intracellular levels measured by ELISA in control, SIRT1 or $SIRT^{1H-Y}$ VSMCs after 1h t-BHP treatment and after 0-24h recovery (*n*=3). **(f)** Western blot of OGG1 expression after CHX (0-4h) treatment of control, SIRT1 or $SIRT^{1H-Y}$ VSMCs (*n*=3). **(g)** Immunohistochemistry for SIRT1, OGG1 or Ac-OGG1 (brown) in aortas from control $ApoE^{-/-}$ or $SIRT1^{-/-}/ApoE^{-/-}$ mice (*n*=10). Tissue sections were also co-stained for αSMA (blue). Negative control sections with isotype-matched antibodies are shown below. Scale bar, 25μm. All graphical data are mean ± SEM, *P< 0.05, ***P< 0.001, one-way ANOVA (Bonferroni post hoc).

Figure. 5 OGG1 regulates 8oxoG expression in VSMCs *in vivo* and BER

(a) Western blot of OGG1, Ac-OGG1 and myc tag in VSMCs cultured from wild type (control), $OGG1^{-/-}$, SM22α-OGG1, or SM22α-$OGG1^{K-R}$ mouse aortas (*n*=4). **(b)** 8oxoG intracellular levels measured by ELISA in Control, $OGG1^{-/-}$, SM22α-OGG1, or SM22α-$OGG1^{K-R}$ VSMCs (*n*=4).

(c) BER assay quantification in Control, OGG1$^{-/-}$, SM22α-OGG1, or SM22α-OGG1^{K-R} VSMCs treated with t-BHP for 1h and recovered for up to 24h (*n*=4). All graphical data are mean ± SEM, *P< 0.05, one-way ANOVA (Bonferroni post hoc).

Figure 6. Effects of OGG1 on plaque development and morphology *in vivo*

(a) Representative images and quantification of *en face* preparations of descending aortas from Control ApoE$^{-/-}$ (*n*=12), OGG1$^{-/-}$ ApoE$^{-/-}$ (*n*=14), SM22α-OGG1 ApoE$^{-/-}$ (*n*=12) and SM22α-OGG1^{K-R} ApoE$^{-/-}$ (*n*=13) mice stained with Oil Red O. Scale bar, 2mm**. (b)** Hematoxylin-eosin (H&E) and Masson's trichome immunohistochemistry of Control ApoE$^{-/-}$ (*n*=12), OGG1$^{-/-}$ ApoE$^{-/-}$ (*n*=14), SM22α-OGG1 ApoE$^{-/-}$ (*n*=12) and SM22α-OGG1^{K-R} ApoE$^{-/-}$ (*n*=13) mouse aortic roots at 22 weeks after fat feeding from 8 to 22 weeks. Quantification of % plaque size, plaque area, core area and cap area (μm^2). Scale bar, 200 μm. All graphical data are mean ± SEM, **P< 0.01, ***P < 0.001, one-way ANOVA (Bonferroni post hoc).

Figure 7. OGG1 regulates DNA strand breaks, cell senescence, apoptosis, and inflammasome pathways

(a) Comet assay with quantification for cultured VSMCs from wild type control, OGG1$^{-/-}$, SM22α-OGG1, or SM22α-OGG1^{K-R} mice treated with t-BHP for 1h and recovered for 6h (*n*=3). Scale bar, 100μm. **(b)** Chromatin immunoprecipitation-qPCR using primers to a telomeric region on 8oxoG-bound chromatin from control, OGG1$^{-/-}$, SM22α-OGG1, or SM22α-OGG1^{K-R} mouse VSMCs (*n*=3). Data are shown as fold-change over IgG. **(c)** % VSMCs expressing senescence-associated beta galactosidase activity (SaβG) from wild type control, OGG1$^{-/-}$, SM22α-OGG1, or SM22α-OGG1^{K-R} mice (*n*=3). **(d)** Apoptosis assayed by Annexin V and

propidium iodide staining of mouse cells ± t-BHP treatment by flow cytometry (*n*=3). **(e)** Relative expression of transcripts for inflammatory cytokines and inflammasome-associated components in aortic arch tissue from Control ApoE$^{-/-}$, OGG1$^{-/-}$ ApoE$^{-/-}$, SM22α-OGG1 ApoE$^{-/-}$ and SM22α-OGG1^{K-R} ApoE$^{-/-}$ mice after fat feeding (n=4). All graphical data are mean ± SEM, *P<0.05, **P<0.01, ***P<0.001, one-way ANOVA (Bonferroni post hoc).

Figure 8. Model of OGG1 regulation in VSMCs in atherosclerosis

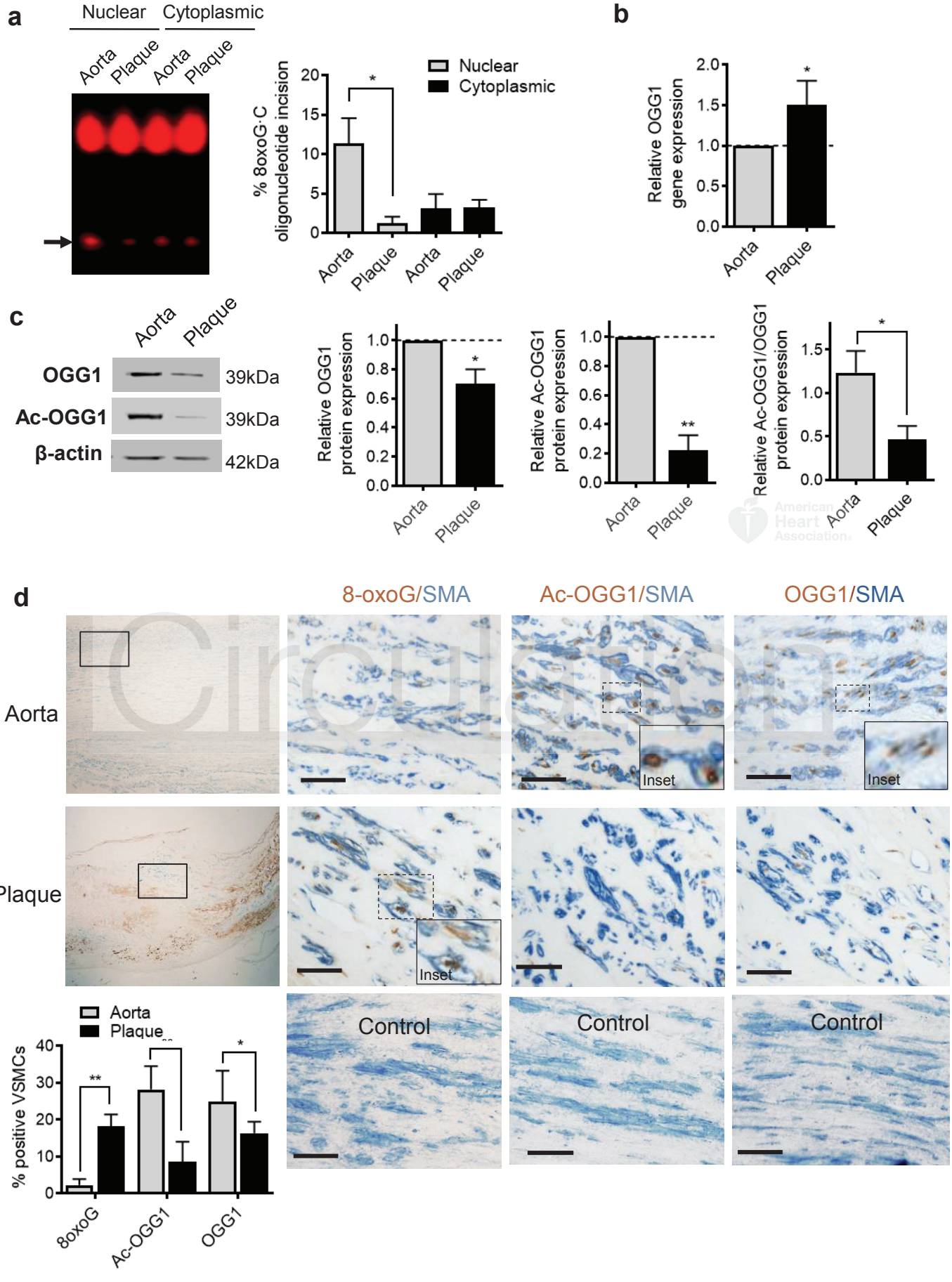

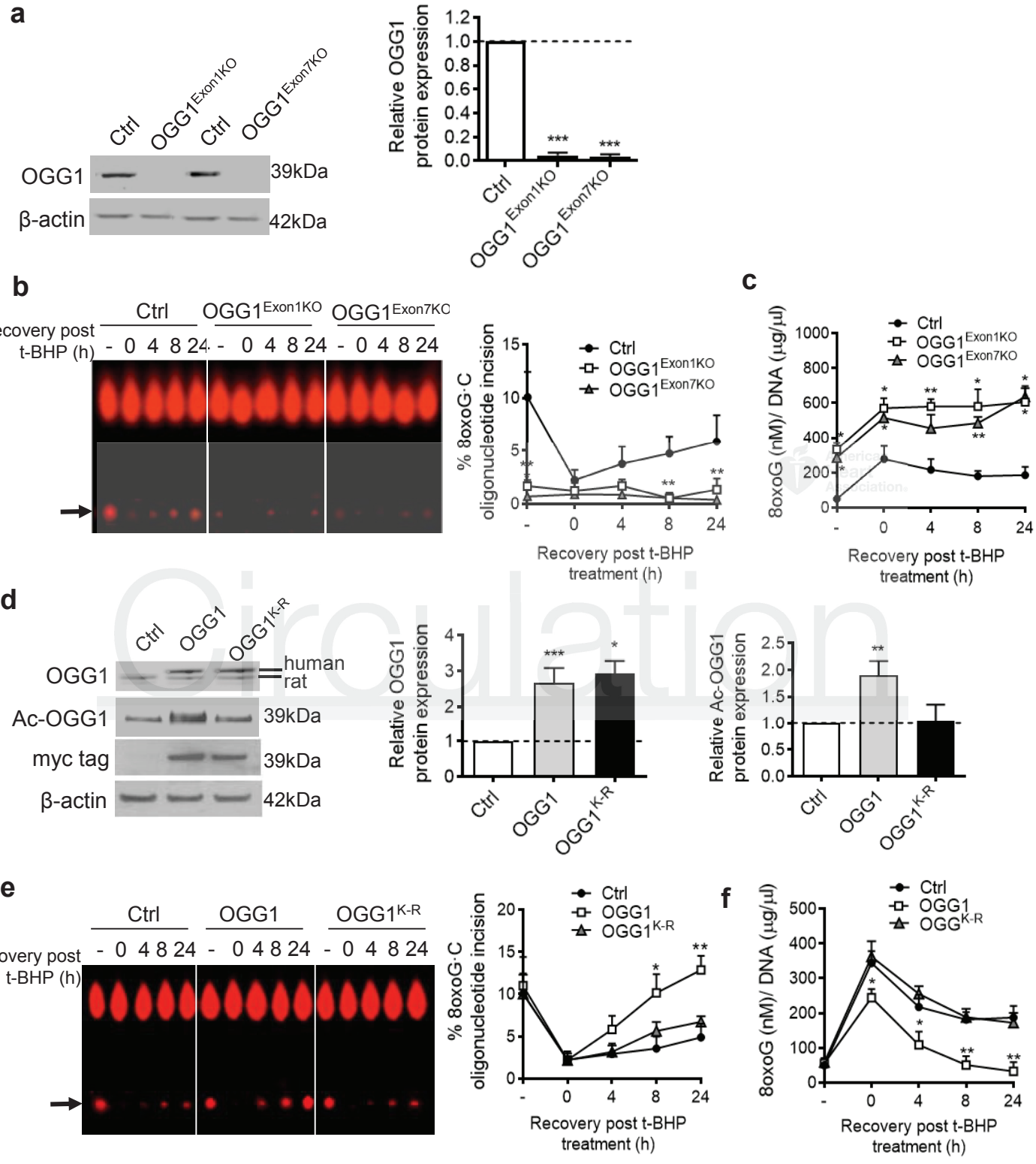

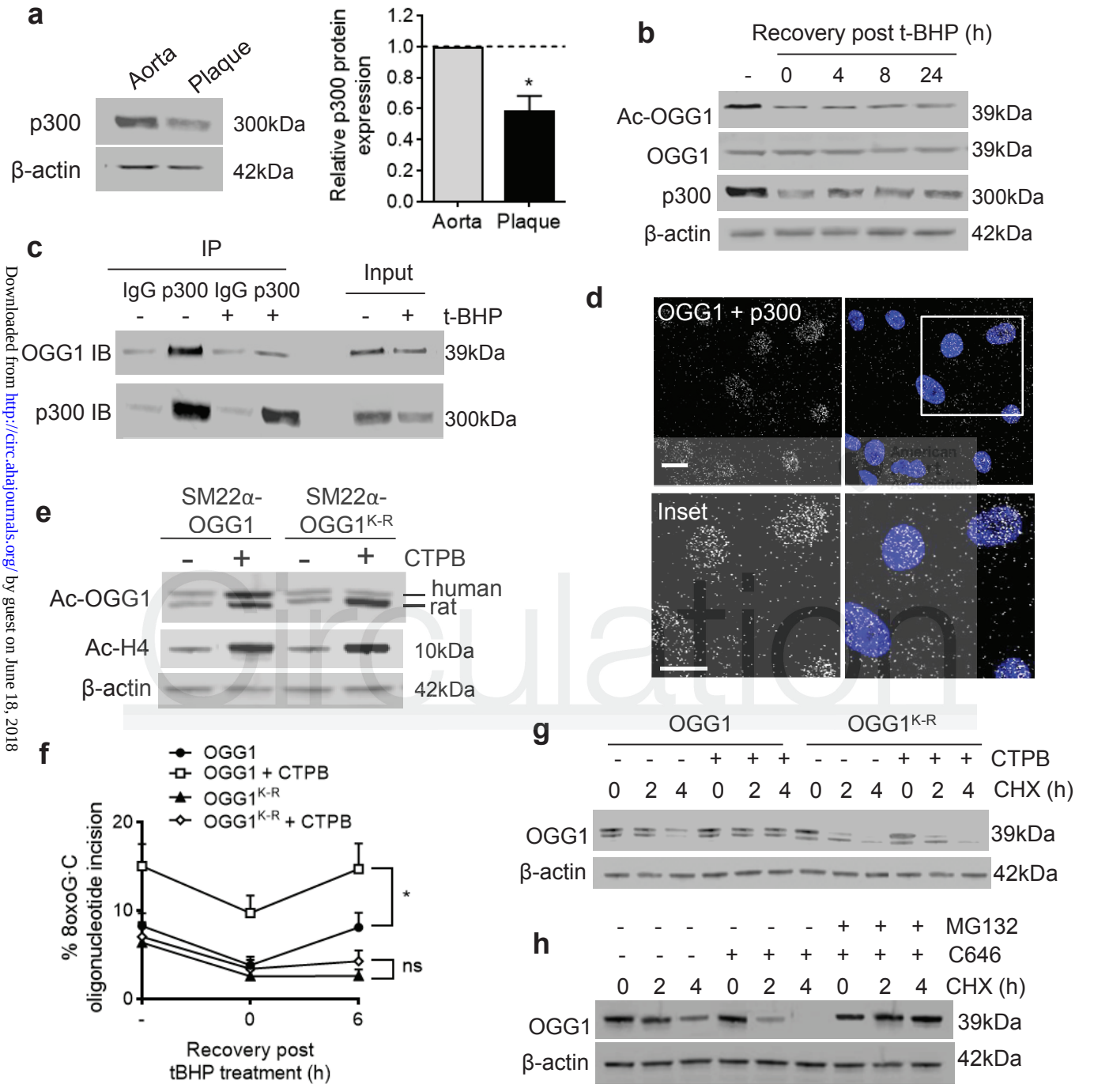

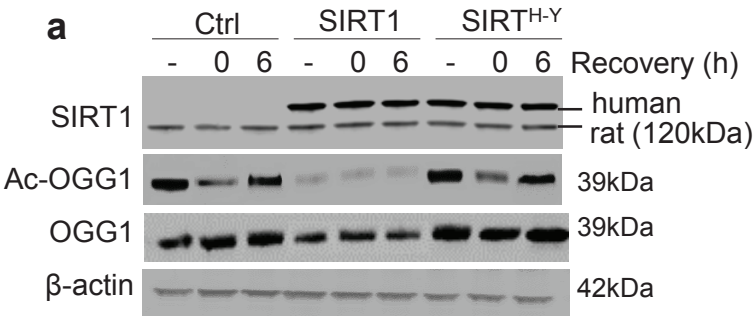

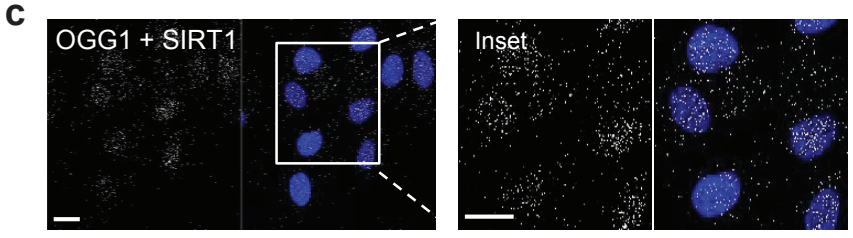

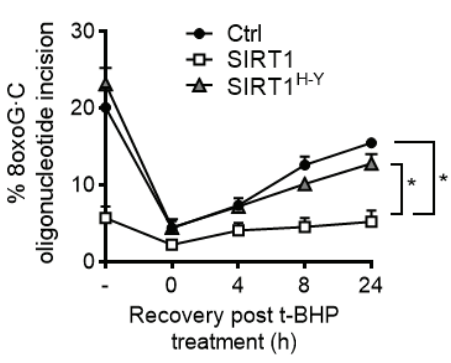

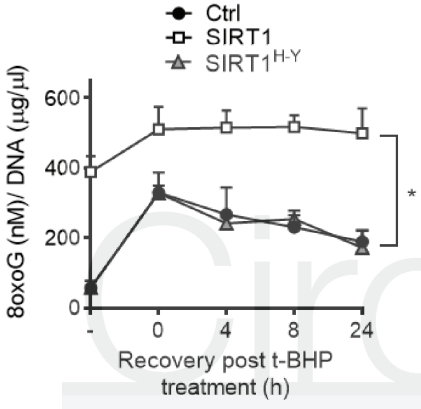

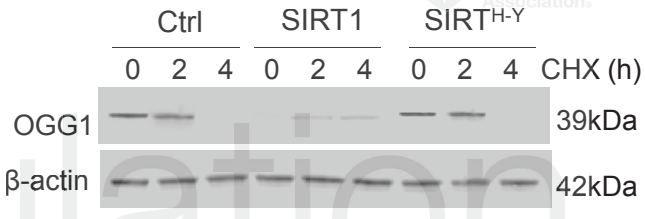

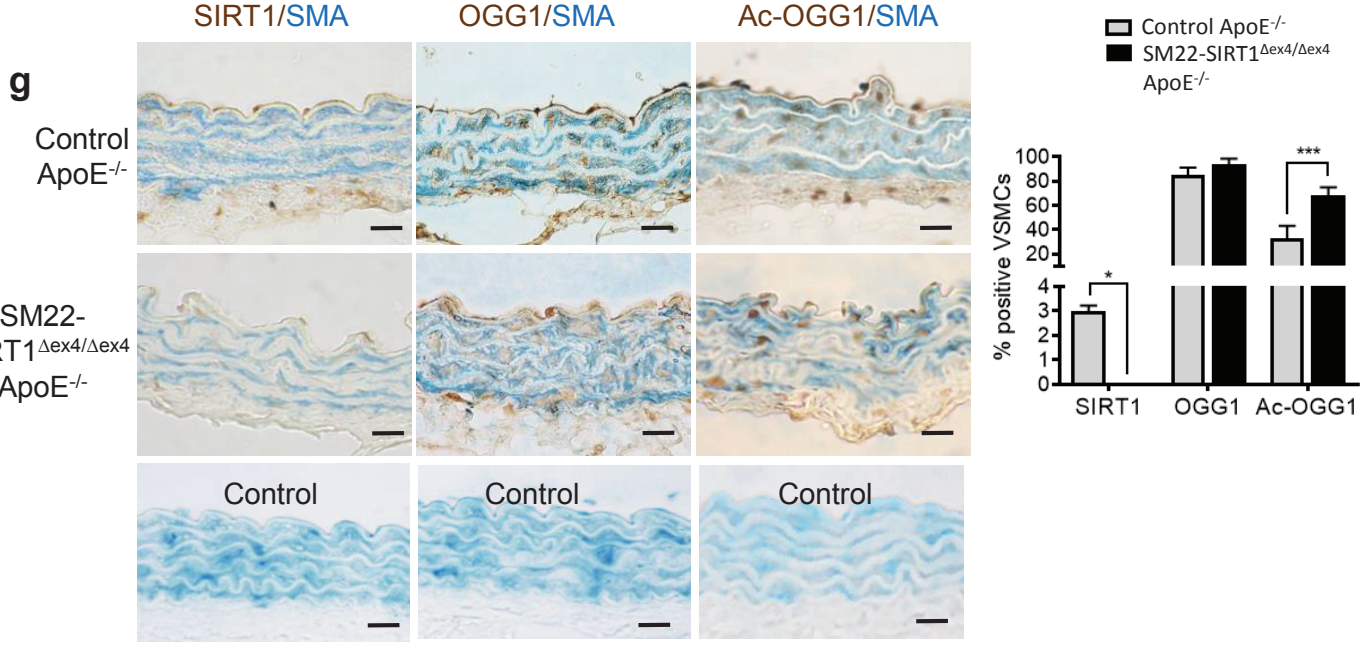

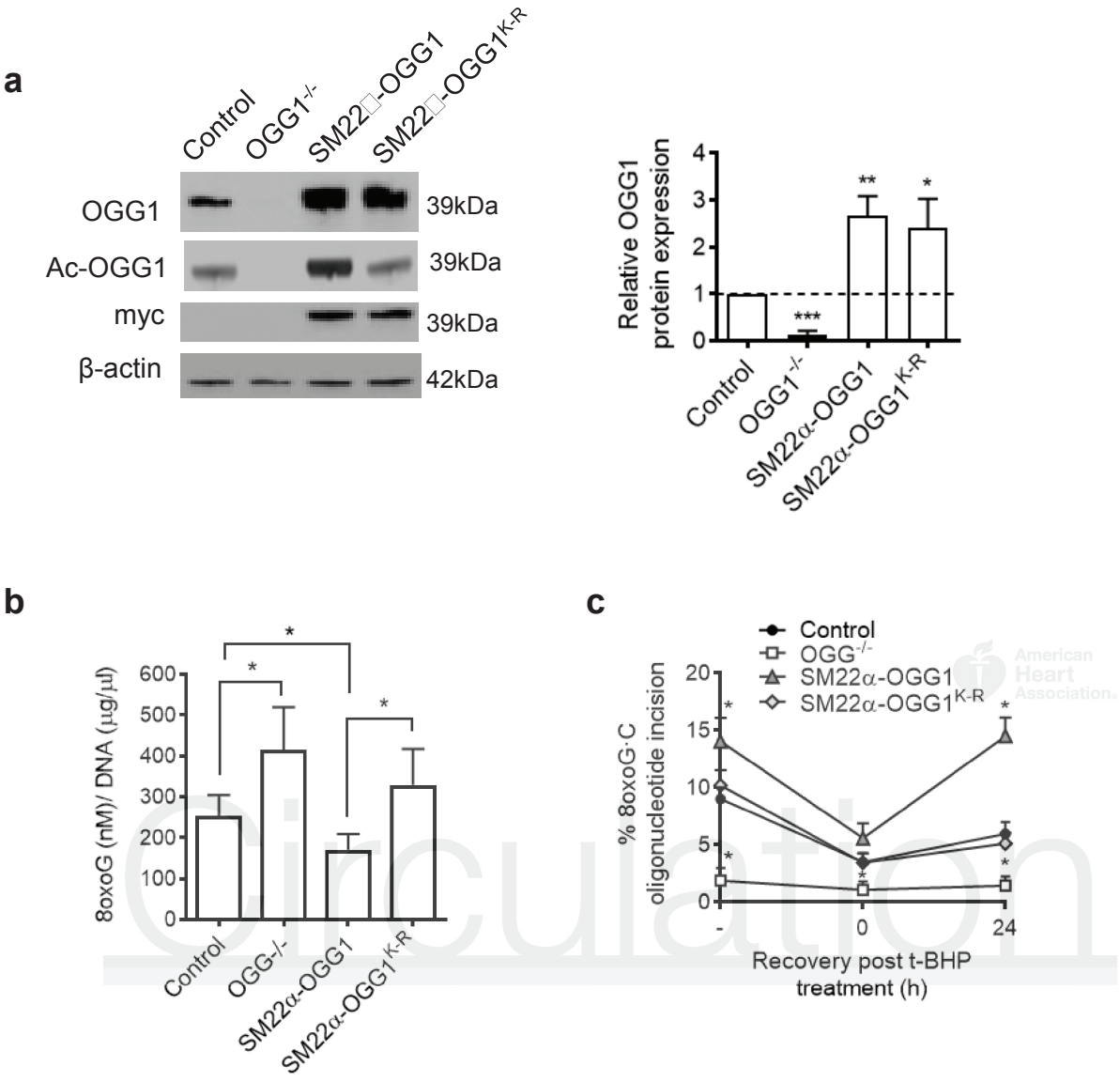

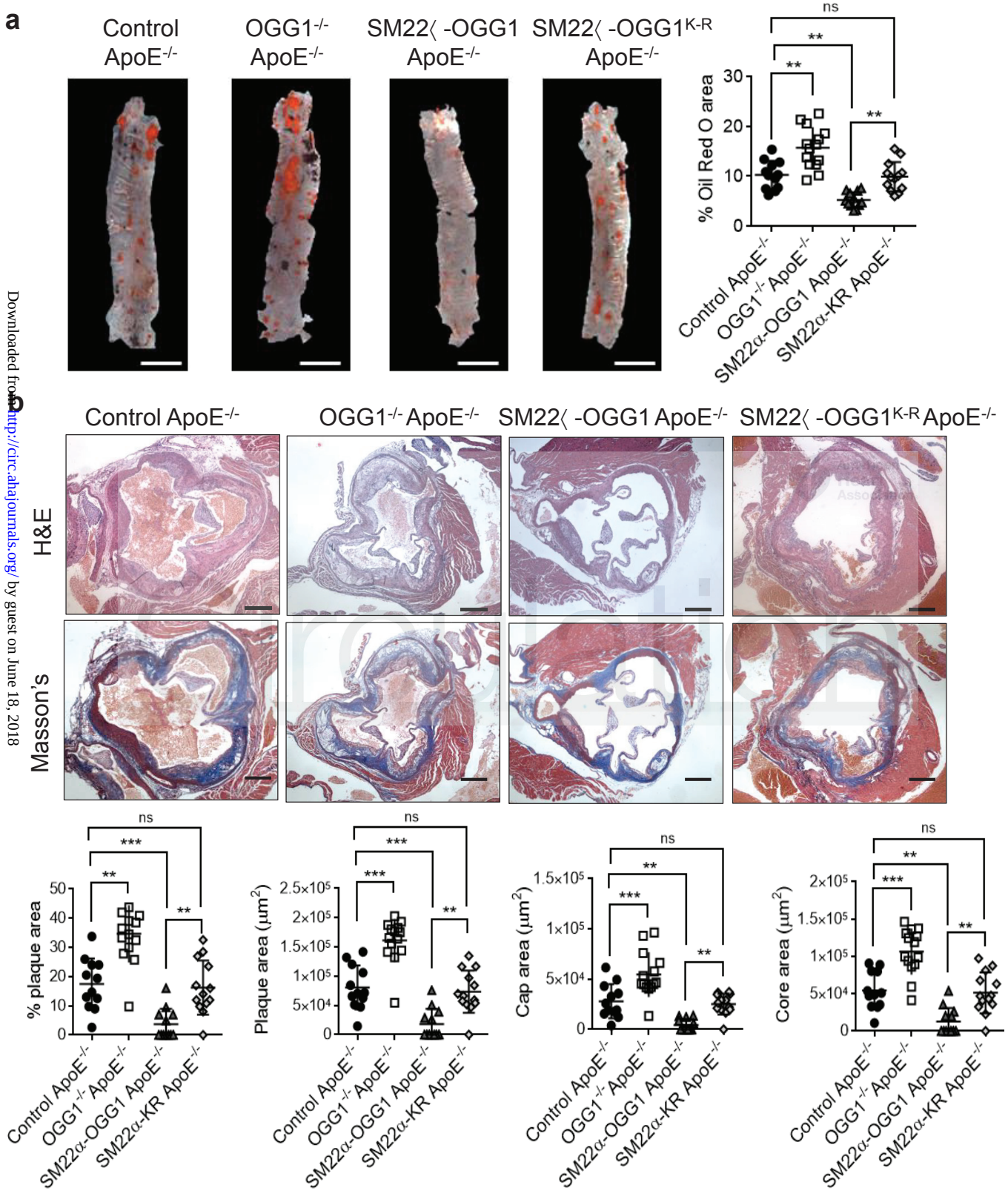

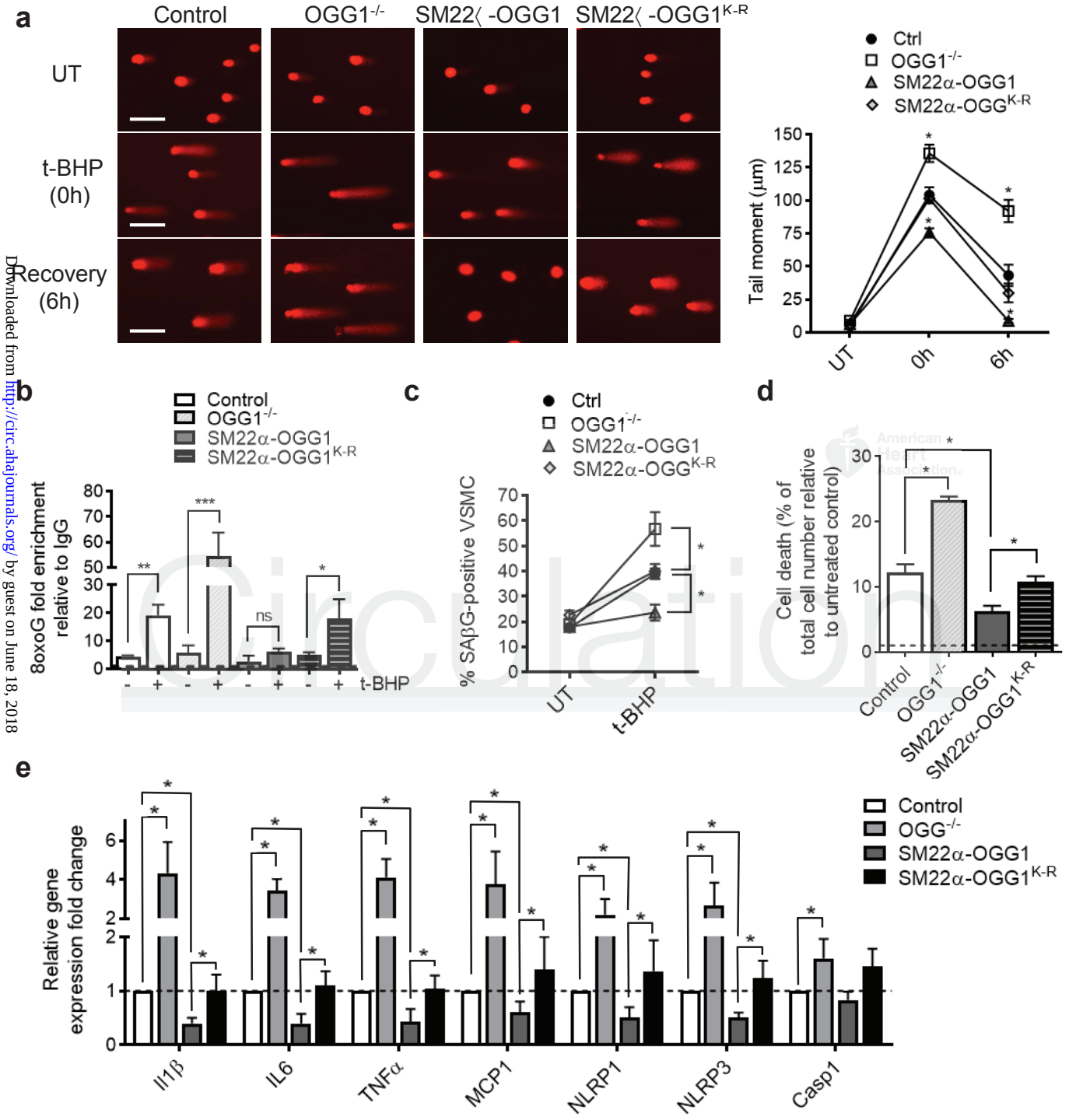

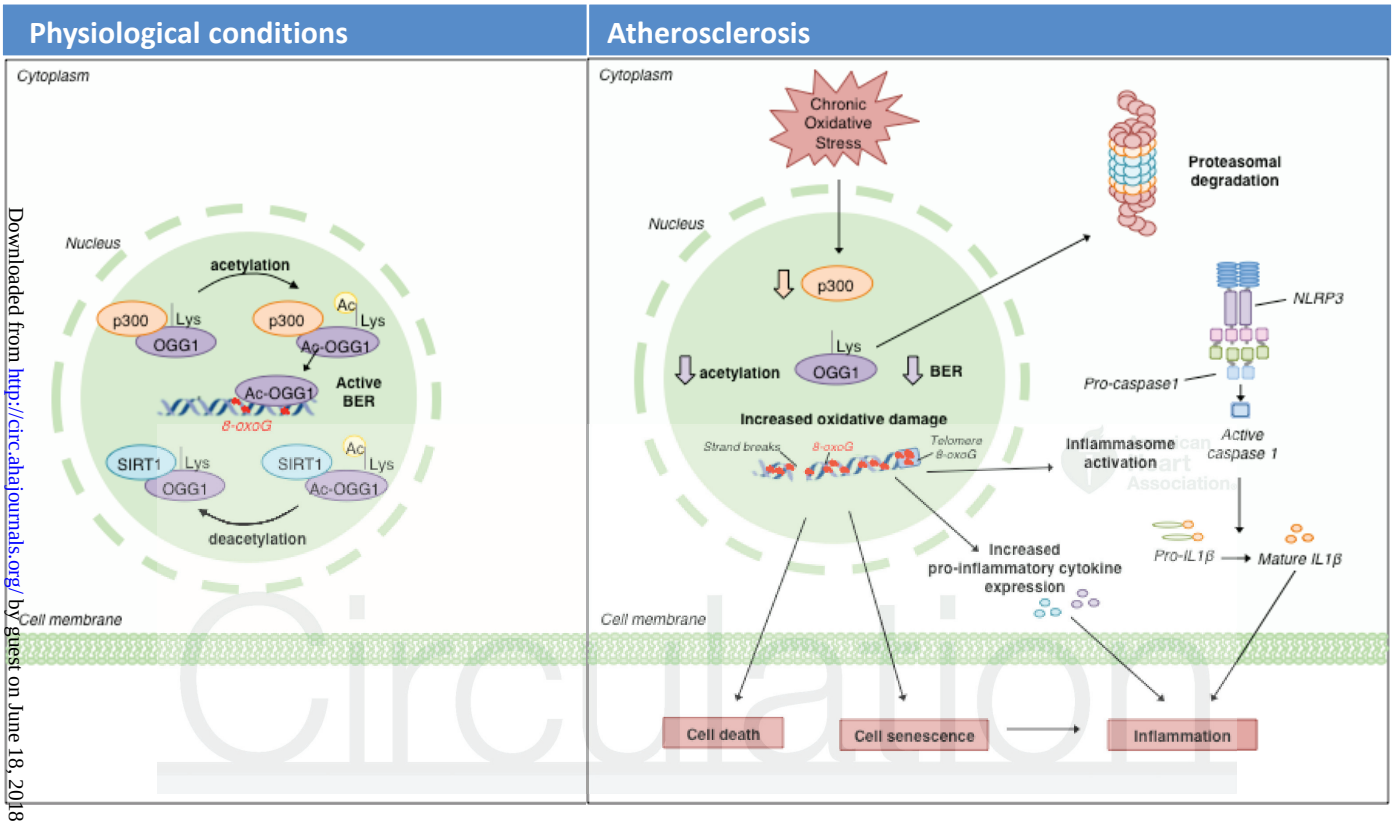

Defective Base Excision Repair of Oxidative DNA Damage in Vascular Smooth Muscle Cells Promotes Atherosclerosis

Aarti Shah, Kelly Gray, Nichola Figg, Alison Finigan, Lakshi Starks and Martin Bennett

Circulation. published online April 11, 2018;
Circulation is published by the American Heart Association, 7272 Greenville Avenue, Dallas, TX 75231

Print ISSN: 0009-7322. Online ISSN: 1524-4539

SUPPLEMENTAL MATERIAL

SUPPLEMENTAL METHODS

Generation of transgenic mice

To produce transgenic mouse targeting constructs, myc-tagged hOGG1 or OGG1^{K-R} cDNA was subcloned between the minimal SM22α promoter and a polyA sequence in pBluescript. The SM22α-OGG1 and SM22α-OGG1^{K-R} transgenes were digested with BssHII and the transgene-containing fragment purified from an agarose gel. Transgenic mice were generated by pro-nuclear injection of SM22α-OGG1 and SM22α-OGG1^{K-R} fragments into C57Bl6 embryos, and positive progeny used to generate individual lines.

Genotyping

Ear notches from transgenic mice were incubated with Chelex/Proteinase K for 2h at 56˚C. Following heat inactivation at 95˚C, 2 µl DNA was used in the subsequent PCR reaction. ApoE$^{-/-}$ genotyping was conducted according to Jackson Labs protocols and cycling conditions: 94˚C for 10 min, followed by 40 cycles of 94˚C for 45s, 63˚C for 45s and 72˚C for 90s. OGG1 genotyping was performed using the following cycling conditions: 95˚C for 5 min, followed by 40 cycles of 95˚C for 1 min, 62˚C for 2 min and 72˚C for 90s. SM22α-OGG1 transgene expression was analysed using primers that amplify a 550 bp region of OGG1 fused to the C-terminal myc tag using the following cycling conditions: 95˚C for 5 min, followed by 40 cycles of 94˚C for 1 min, 57˚C for 1 min and 72˚C for 1 min. PCR products were analysed on a 2% agarose gel containing ethidium bromide. Oligonucleotide sequences used for genotyping are listed in **Supplementary Table S1**.

For heterozygosity genotyping, digested ear notches were diluted 1:10 and underwent standard 2 step qPCR (Rotor-gene Q). Briefly, 3µl DNA was used in a qPCR reaction containing 2x PCR mastermix (Life Technologies), 20x human OGG1 or mouse GAPDH Taqman primer-probes (Life Technologies) and H_2O. Samples were analysed for OGG1 gene expression and normalized to GAPDH expression. Heterozygosity was defined by analysing the OGG1:GAPDH ratio whereby no expression corresponded to null animals; heterozygous animals had gene expression at 50% of the value of homozygous-positive animals.

Blood pressure analysis and cytokine detection

Blood pressure was determined by tail cuff measurements. V-PLEX Mouse Proinflammatory Panel 1 and U-PLEX Chemokine Combo immunoassays (Meso Scale Discovery, Maryland, USA) were used to determine cytokine concentrations in conditioned media from cell lines or mouse serum. Samples were analyzed according to the manufacturer's recommendations.

Oil Red O staining of descending aorta

Oil Red O (0.2 g, Sigma) was dissolved in 100 ml of isopropanol and filtered through Whatman No. 1 filter paper (stock solution). The working stain was prepared by diluting the stock solution with distilled water (6:4). Adventitial tissue was carefully removed from the descending aorta, the artery opened along the longitudinal axis, rinsed in distilled water, rinsed in 60 % isopropanol for 30 sec, stained with Oil Red O working stain for 15 min, rinsed again in isopropanol and returned to distilled water. The vessel was laid flat on a glass slide, mounted in water, covered with a coverslip and imaged *en face* using an Olympus BX51 microscope equipped with an Olympus Lumenera Infinity 3 digital camera and analyzed using ImageJ software. The percentage of the luminal surface area stained by Oil Red O was determined.

Histological Analysis

Atherosclerosis extent and composition was analyzed as described previously[9]. Briefly, sections from the aortic root were stained with Haematoxylin and Eosin (H&E), Masson's,

8oxoG and TUNEL. Plaque extent and composition was measured using ImageJ analysis software with an observer blind to experimental group. SMA content of fibrous caps was defined using Masson's Trichrome to identify the fibrous cap region. Fibrous caps were defined as the area rich in VSMCs and proteoglycan overlying the cholesterol-rich, matrix-poor, acellular regions of the necrotic cores. Very small plaques (<90,000μm^2) were not included in the above analysis since it was impossible to demarcate a fibrous cap.

Cell culture
Human, rat and mouse VSMCs were cultured in Dulbecco's modified Eagle's medium (DMEM, Sigma) supplemented with 100 U/ml penicillin, 100 μg/ml streptomycin, 2 mM L-glutamine, and 10 % FCS.

Human VSMCs were cultured from explants. The endothelial layer was removed using a scalpel and tissue cut into 2-3mm² pieces, placed into 6-well plates containing 1ml media and grown for 1-2 weeks to allow cells to emerge. Human VSMCs were studied at passages 2–5; VSMC cultures from individual patients were not pooled. Rat and mouse aortic VSMCs were prepared by removing surrounding tissues and enzymatic dispersion using Type I collagenase (1 mg/ml, Sigma) and elastase (0.5 mg/ml, Worthington Biochemical) in serum-free medium for 1h at 37 °C.

Cells were treated with tert-butyl hydrogen peroxide (t-BHP, Sigma), C646 (Sigma), CTPB (Sigma), cycloheximide (Sigma) or MG132 (Sigma) as indicated in figure legends.

Transfections and virus infections
Retrovirus infection was used to produce stable expression of wild type OGG1 or the acetylation mutant OGG1$^{K\text{-}R}$ in rat aortic VSMCs. hOGG1 was subcloned from pCMV-myc-Nuc-hOGG1 (Addgene) and site-directed mutagenesis performed using the QuikChange Lightning Multi Site-Directed Mutagenesis Kit (Stratagene) following the manufacturer's instructions.

pBabe-puro vectors encoding human OGG1 or OGG1$^{K\text{-}R}$ were used to transfect Phoenix^{TM} packaging cells (Orbigen) using SuperFect (Qiagen). Virus-producing cells were selected with hygromycin B (300 μg/ml; Calbiochem). VSMCs were infected with the virus suspension in the presence of 8 μg/ml Polybrene (hexadimethrine bromide, Sigma), and selected with 5 μg/ml of puromycin (Sigma).

CRISPR-mediated gene silencing
For gene silencing experiments, rat aortic VSMCs were transfected with a U6-gRNA/CMV-Cas9-GFP CRISPR plasmid targeting OGG1 (Sigma). To generate rat OGG1$^{-/-}$ VSMCs, cells were trypsinized 3 days after transfection and resuspended in PBS with 0.1% BSA and 2 mM EDTA. Single GFP-positive cells were sorted by FACS into 96-well plates, and clonal cell populations expanded. OGG1 protein expression of each clone was examined by immunoblotting, and clones with efficient OGG1 knockout used for further studies. Genomic DNA was extracted from 1 × 10^6 cells, and locus-specific cleavage was analyzed using the GeneArt Genomic Cleavage Detection Kit (Life Technologies).

Real-time polymerase chain reaction
RNA extraction from mouse tissues and primary VSMCs was performed using the RNeasy kit (Qiagen). First strand cDNA synthesis was performed using Superscript III Reverse Transcriptase (Invitrogen). Quantitative real-time PCR was performed using Rotor-Gene SYBR Green PCR Kit (Qiagen) on a Rotor-Gene 6000 QPCR thermocycler (Corbett Research). Oligonucleotide sequences used are listed in **Supplementary Table S1**.

Oligonucleotide incision assay

8oxoG BER activity in nuclear lysates was determined using a 40-mer oligonucleotide containing an 8oxoG at position 19 and labelled at the 3' end with indodicarbocyanine (5'-AGAGAAGAAGAAGAA(G*)AGATGGGTTATTCGAA-CTAGC-Cy5Sp-3'). This oligonucleotide was hybridized to its complementary sequence containing a cytosine opposite the 8oxoG lesion (G*). Nuclear extracts were added to a 10μL standard incision reaction mixture containing 200 fmoles of the 8oxoG:C-labeled duplex in 20 mmol/L Tris–HCl (pH 7.1), 1 mmol/L EDTA, 200 mmol/L NaCl, 1 mg/mL bovine serum albumin (BSA), and 5% glycerol. After 15 min at 37°C, the incision reaction was stopped by adding 4 μL of formamide dye and heating for 5 min at 95°C. The cleaved product was separated from the intact substrate in a 20% polyacrylamide gel containing 8 M urea in Tris-borate-EDTA buffer, pH 8.4. Fluorescence in the separated DNA bands was visualized using a LI-COR Odyssey CLx system.

8oxoG ELISA
Cell lysates were assessed for 8oxoG expression using a competitive ELISA assay (Abcam) as per the manufacturer's instructions. Total DNA was purified from VSMC lysates by using the DNeasy Blood & Tissue Kit (Qiagen). DNA was digested using nuclease P1 following the manufacturer's instructions. The pH was adjusted to 7.5-8.5 using 1M Tris and 1 unit alkaline phosphatase added per 100 μg DNA and incubated at 37°C for 30 minutes. Samples were boiled for 10 min and placed on ice until use. Absorbance was measured on a Synergy HT Plate Reader (Biotek) with standard curves generated from known concentrations of 8oxoG standards.

Intracellular ROS measurement
Intracellular ROS was measured by using the oxidant-sensitive fluorescent probe 5-(and-6)-chloromethyl-2',7'-dichlorodihydrofluorescein diacetate acetyl ester (CM-H2DCFDA,10 mM; Molecular Probes). Cells were incubated continuously with CM-H2DCFDA during experimental conditions. Subsequently, cells were washed and lysed in 0.1% Triton X-100. Fluorescence was measured in the Biotek synergy HT plate reader with excitation of 488 nm and emission of 530 nm.

Annexin V/PI flow cytometry
Cell death was determined using an Apoptosis Detection kit according to the manufacturer's instructions (BD BioSciences). Briefly, cells (1×10^5 cells/sample) were washed twice in cold PBS and suspended in binding buffer containing fluorescein isothiocyanate-conjugated annexin V (10 μg/ml) and PI (10 μg/ml). The cell suspension was incubated in the dark for 15 min and fluorescence measured using an Accuri C6 flow cytometer (BD Biosciences). A total of 10,000 events were analyzed for each sample with Cell Quest software (BD Biosciences).

Comet assay
5×10^4 VSMCs were washed with PBS, resuspended in 150 μl 1% low melting point agarose (LMPA) and left to cool on Gel-bond films (Trevigen) at 4˚C for 10 min to set the agarose. Gel-bond films were incubated overnight in lysis buffer at 4˚C, washed briefly with water, and placed in alkaline electrophoresis buffer for 30 min prior to electrophoresis at 26V for 30 min at 4˚C. Gel-bond films were washed in neutralization buffer (100 mM Tris pH 7.6) and subsequently immersed in ice-cold ethanol for 10 min. Films were dried overnight, rehydrated in distilled H_2O for 10 min and stained with 2μg/ml ethidium bromide (Sigma) solution in the dark at RT for 2 h. Multiple images per slide were analysed using a Zeiss microscope and comet tail length/moment measured using Comet Assay IV software (Perception Instruments).

Immunofluorescence
VSMCs for immunofluorescence and Proximity Ligation Assay (PLA) were cultured in chamber slides (ThermoFisher Scientific), fixed with 4 % paraformaldehyde for 15 min and

permeabilized for 5 min with 0.5% Triton X-100 in PBS prior to blocking with 3% BSA for 1 h. For immunofluorescence, cells were incubated with the following primary antibodies: rabbit anti-acetyl OGG1 (1:200, ab93670, Abcam) and rabbit anti-myc tag (1;1000, 2272S, Cell Signaling). Secondary antibodies were anti-rabbit Alexa Fluor 568, anti-mouse Alexa Fluor 568 and anti-mouse Alexa Fluor 594 (1:1000, Invitrogen). Nuclei were visualized using DAPI. PLA was performed according to manufacturer's instructions using the Duolink® In Situ Red Kit Mouse/Rabbit (Sigma) and the following primary antibodies: rabbit-anti OGG1 (1:200, PA1-16505, Thermofisher), mouse anti-p300 (1:100, NB100-616, Novus) and mouse anti-SIRT1 (1:100, 8469S, Cell Signaling). Nuclei were visualized using DAPI. Slides were mounted with DAPI-containing medium (Sigma or Vectashield, Vector Labs) and visualized with a BX51 fluorescent microscope (Olympus).

Immunoprecipitation
VSMCs were harvested in RIPA lysis buffer (20 mM Tris-HCl pH7.5, 150 mM NaCl and Triton 0.5 %) supplemented with protease and phosphatase inhibitor cocktails (Sigma). After clarification by centrifugation, 800 µg of total protein cell lysate was incubated with 4 µg of rabbit anti-OGG1 antibody (PA1-16505, Thermofisher) overnight at 4 °C. Immuno-complexes were precipitated with Pierce protein A/G magnetic beads for 4h at 4°C and detected by western blot with goat anti-OGG1 (PA5-18747, 1:500, Thermofisher), mouse anti-p300 (RW128, 1:500, Millipore), or mouse anti-SIRT1 (8469S, 1:1000, Cell Signaling) antibodies. Primary antibodies were detected using HRP-conjugated secondary antibodies and chemiluminescence (Amersham ECL or ECL prime reagents) detection.

Western blotting
Whole cell protein lysates were prepared using CelLytic reagent (Sigma). Immunoblotting of cell lysates was performed according to standard conditions. Immunoblots were labelled with the following primary antibodies: rabbit anti-acetyl histone 4 (1:1000, 06-866, Millipore), rabbit anti-acetyl OGG1 (1:1000, ab93670, Abcam), rabbit anti-myc tag (1;1000, 2272S, Cell Signalling, rabbit anti-NEIL1 (1:1000, ab128294, Abcam), mouse anti-NTH1 (1:500, ab70726, Abcam), rabbit anti-OGG1 (1:1000, ab124741, Abcam), mouse anti-p300 (1:500, RW128, Millipore), mouse anti-SIRT1 (1:1000, 8469S, Cell Signaling). Primary antibodies were detected using fluorescently labelled secondary antibodies: goat anti-rabbit IgG DyLight 680 and goat anti-mouse IgG Dylight 800 (Thermo Scientific). Detection and quantification of fluorescence intensity were performed using an Odyssey® CLx imaging system (LI-COR Biosciences, Lincoln) and Odyssey® 2.1 software. In some instances, HRP-conjugated secondary antibodies were used for chemiluminescence detection and protein levels quantified by densitometry and normalized against loading controls.

ChIP-qPCR
ChIP was performed using the ChIP-IT express kit (Active Motif), VSMCs were crosslinked for 10 min with formaldehyde (to a final concentration of 1 %). Chromatin was sheared using a Bioruptor UCD-200 ultrasound sonicator (Diagenode), resulting in DNA fragments of 500–1000 bp in size. Chromatin was immunoprecipitated with 2 µg mouse anti-8oxoG antibody (MAB3560, Millipore) or negative control mouse IgG (PP64, Millipore). Immunoprecipitated DNA was then used as a template for quantitative PCR using primers specific for genomic loci. Oligonucleotide sequences used are listed in Supplementary Table S1.

Supplemental Tables

Primers		Oligonucleotide Sequences
CASP1 (mouse)	Forward	5'- GCCCACCACTGAAAGAGTGA -3'
	Reverse	5'- TCTTCACTTCCTGCCCACAG-3'
CCL2 (mouse)	Forward	5'- AGCTGTAGTTTTTGTCACCAAGC -3'
	Reverse	5'- GTGCTGAAGACCTTAGGGCA -3'
GAPDH (human)	Forward	5'- GATGCCCCCATGTTCGTCAT-3'
	Reverse	5'- TGCAGGAGGCATTGCTGATG-3'
GAPDH (mouse)	Forward	5'- GGGTCCCAGCTTAGGTTCATC-3'
	Reverse	5'- CCCAATACGGCCAAATCCGT-3'
HPRT (mouse)	Forward	5'- ACAGGCCAGACTTTGTTGGA-3'
	Reverse	5'- TGCAGATTCAACTTGCGCTC-3'
NLRP1 (mouse)	Forward	5'- TGGTTCAGGGATGCTGGAAA-3'
	Reverse	5'- GCTGCTGGGCACTAGTATCTC-3'
NLRP3 (mouse)	Forward	5'- TCCTGGCTGTAACATTCGGAG-3'
	Reverse	5'- TGCAAGATCCTGACAACATGC-3'
Il1b (mouse)	Forward	5'- GCCACCTTTTGACAGTGATGAG-3'
	Reverse	5'- GACAGCCCAGGTCAAAGGTT-3'
IL6 (mouse)	Forward	5'- GACAAAGCCAGAGTCCTTCAGA-3'
	Reverse	5'- TGTGACTCCAGCTTATCTCTTGG -3'
IL18 (mouse)	Forward	5'- TCTTGGCCCAGGAACAATGG-3'
	Reverse	5'- ACAGTGAAGTCGGCCAAAGT-3'
OGG1 human	Forward	5'- GACTACAGCTGGCACCCTAC-3'
	Reverse	5'- CACTGAACAGCACCGCTTG-3'
OGG1 (genotyping mouse)	Forward	5'- GAGACACATCTTGCAGGGAGC-3'
	Reverse	5'- ACTCAGGACCTTCAGAAGAGCA-3'
	Neo	5'- GATGGATACTTTCTCGCAGG-3'
OGG1 (mouse)	Forward	5'- CCACCCTAGAGGAGCTGGAA-3'
	Reverse	5'- CAGCAGTCTCACACCTTGGA-3'
P300 (human)	Forward	5'- GCAGTGTGCCAAACCAGATG-3'
	Reverse	5'- CATAGCCCATAGGCGGGTTG-3'
SIRT1 (human)	Forward	5'- GGGCTGCGGTTCCTACTG-3'
	Reverse	5'- CAGACACCTATCCGTGGCCT-3'
Telomere ChIP	Forward	5'- GGTTTTTGAGGGTGAGGGTGAGGGTGAGGGTGAGGGT-3'
	Reverse	5'- TCCCGACTATCCCTATCCCTATCCCTATCCCTATCCCTA-3'
TNFα (mouse)	Forward	5'- GATCGGTCCCCAAAGGGATG -3'
	Reverse	5'- CCACTTGGTGGTTTGTGAGTG-3'

Supplemental Table I Oligonucleotides used in this study

Supplemental Figures and Figure Legends

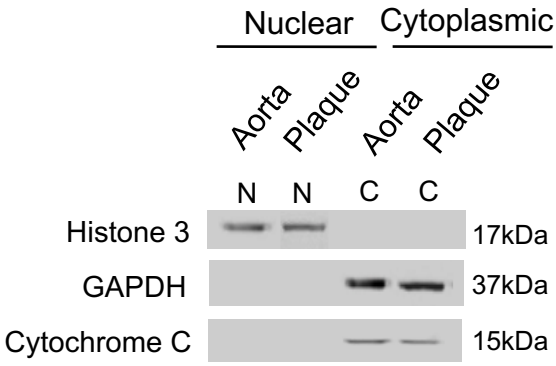

Supplemental Figure I
Western blot analysis for the nuclear marker histone H3, cytoplasmic marker GAPDH, and mitochondrial marker cytochrome c in nuclear or cytoplasmic subfractions of human plaque or normal aortic VSMCs (*n*=3).

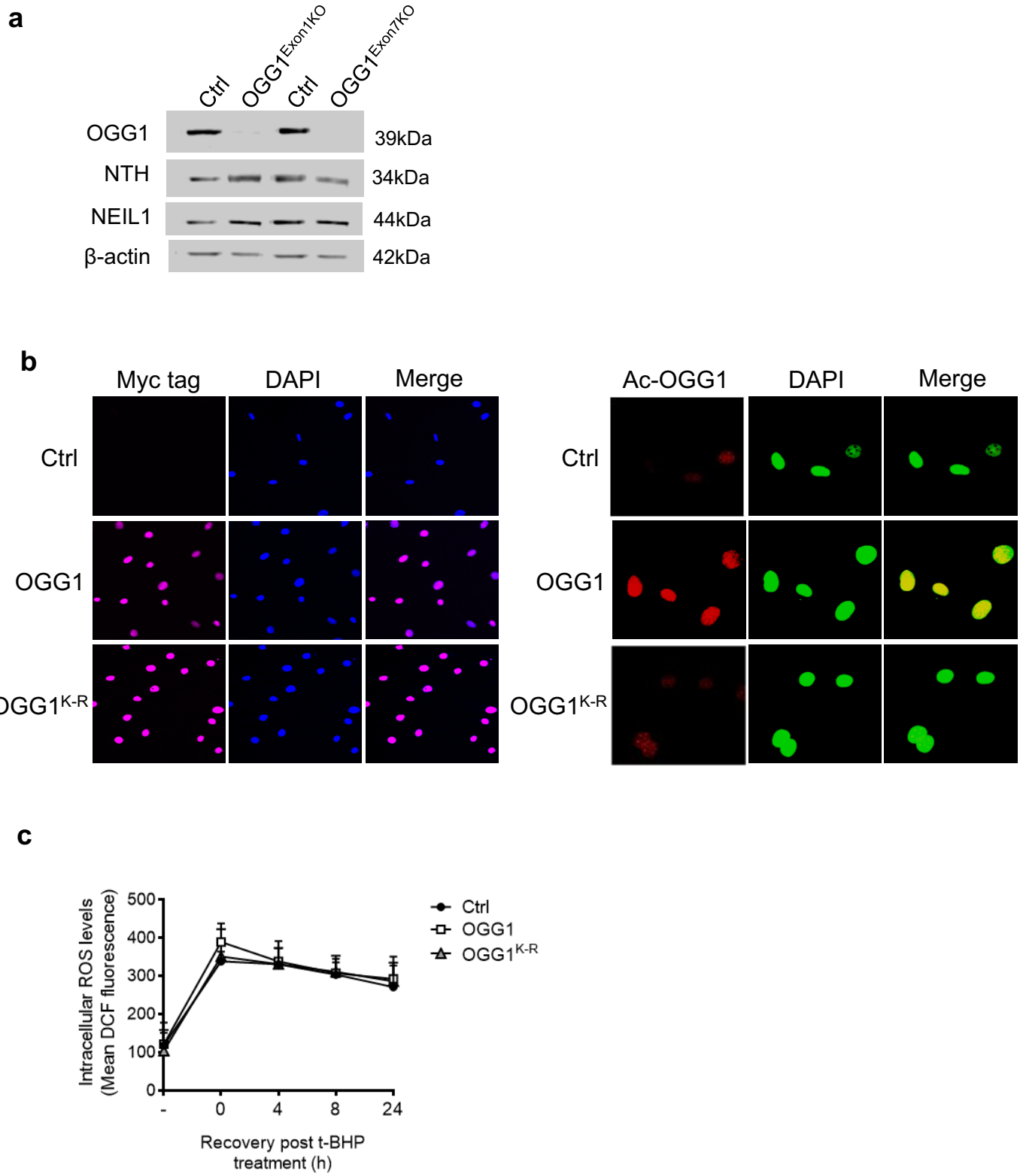

Supplemental Figure II

(**a**) Western blot analysis for OGG1, NEIL1 and NTH1 in Control (Ctrl), OGG1^{Exon1KO} and OGG1^{Exon7KO} rat VSMCs (n=4). (**b**) Immunofluorescence analysis of transgene expression (myc tag; left panel) or Ac-OGG1 (right panel) in VSMCs expressing the empty vector (Ctrl), OGG1 or OGG1^{K-R} (n=3). (**c**) Quantification of intracellular ROS levels in Ctrl, OGG1 or OGG1^{K-R} VSMCs measured by DCFDA fluorescence (n=3).

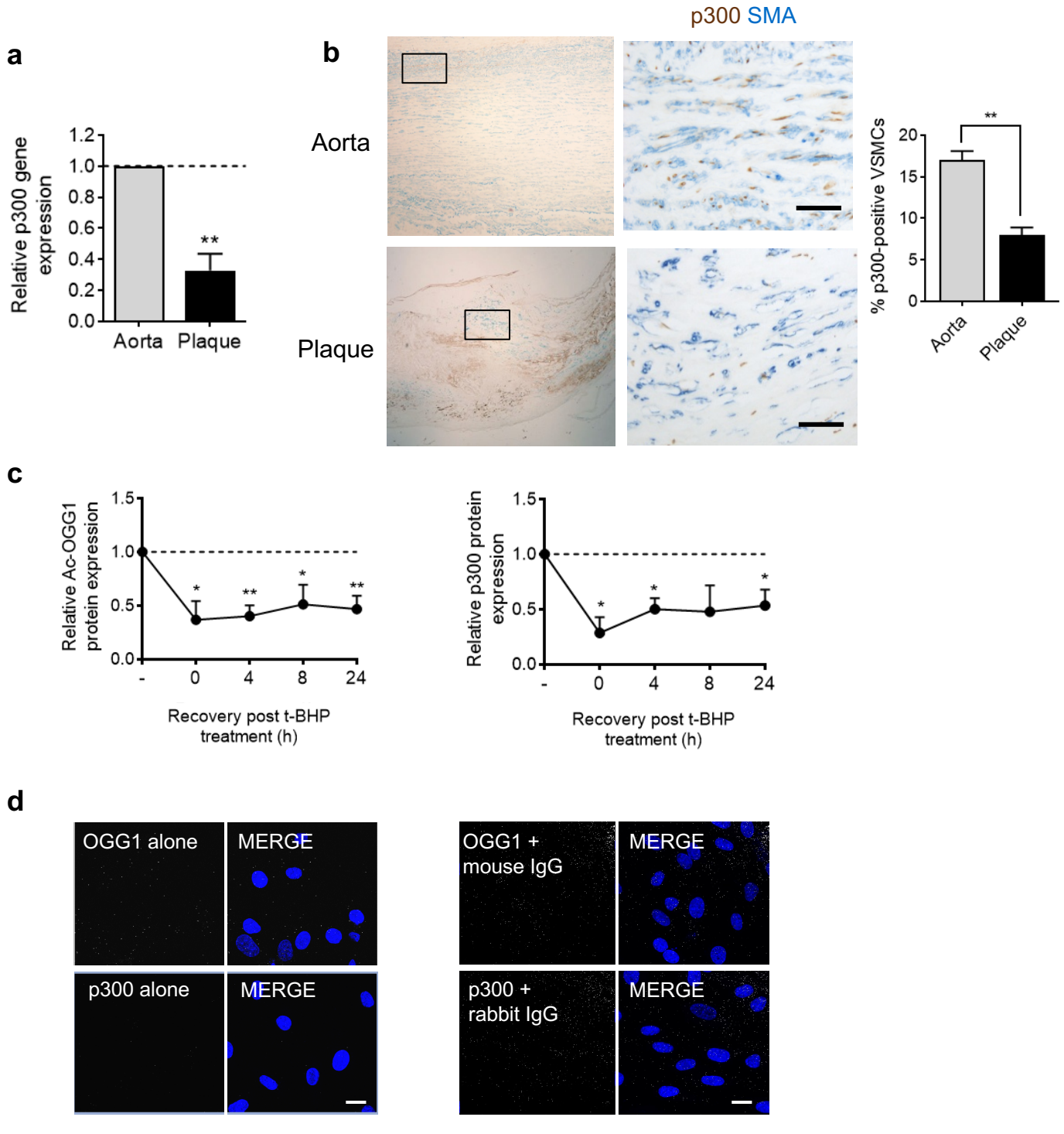

Supplemental Figure III

(a) qPCR analysis of p300 expression in cultured human plaque or normal aortic VSMCs (*n*=4). **(b)** Immunohistochemistry analysis and quantification of p300 (brown) and αSMA (blue) staining in tissue sections of human plaques and normal aorta (*n*=10). High power magnification views of areas outlined on left are shown and quantification. Scale markers, 25μm. **(c)** Quantification of relative Ac-OGG1 and p300 protein expression after t-BHP treatment and 0-24h recovery in control VSMCs (*n*=3). **(d)** Negative control PLA analysis using rabbit anti-OGG1 and mouse anti-p300 antibodies alone or with mouse IgG and rabbit IgG respectively (*n*=3). All graphical data are mean ± SEM, *P< 0.05, **P< 0.01, Student's t-test.

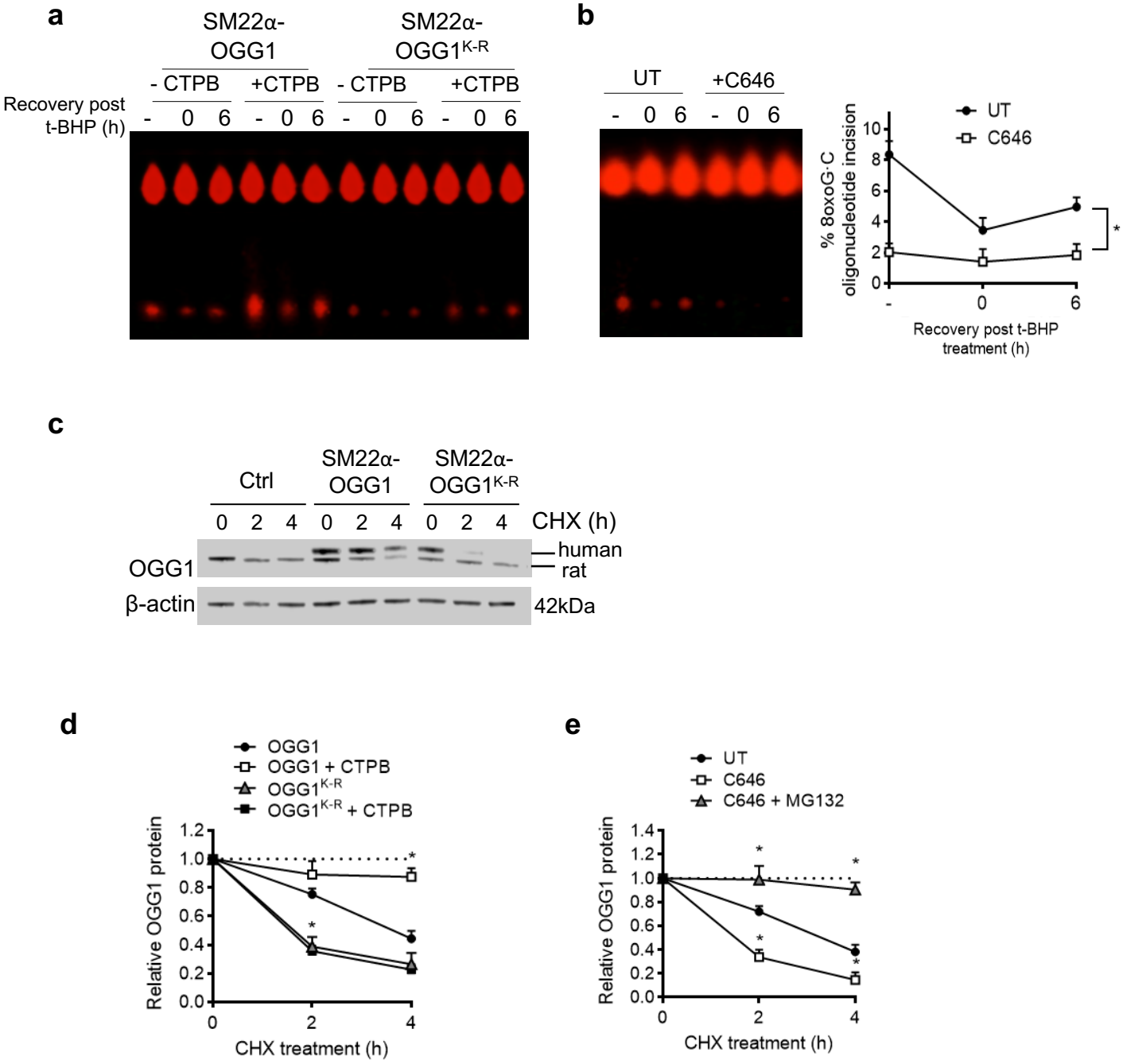

Supplemental Figure IV

(a) Representative BER assay in SM22α-OGG1 and SM22α-OGG1^{K-R} mouse VSMCs (left) ±CTPB (10μM) after 1h t-BHP treatment and 0- 6h recovery (*n*=3). **(b)** BER assay and quantification in control VSMCs either untreated (UT, -), after 1h t-BHP (0) or 6h recovery ± C646 (10μM) (*n*=3). **(c)** Western blot showing levels of OGG1 after CHX treatment in Ctrl, OGG1 or OGG1^{K-R} VSMCs (*n*=4). **(d)** Quantification of Western blot in Figure 3g showing levels of OGG1 after CHX treatment in OGG1 or OGG1^{K-R} VSMCs ±CTPB (*n*=3). **(e)** Quantification of Western blot in Figure 3h of OGG1 levels after CHX treatment in control VSMCs ± p300 inhibitor C646 and MG132 (10μM) (*n*=3). All graphical data are mean ± SEM, *P< 0.05, Student's t-test or one-way ANOVA (Bonferroni post hoc).

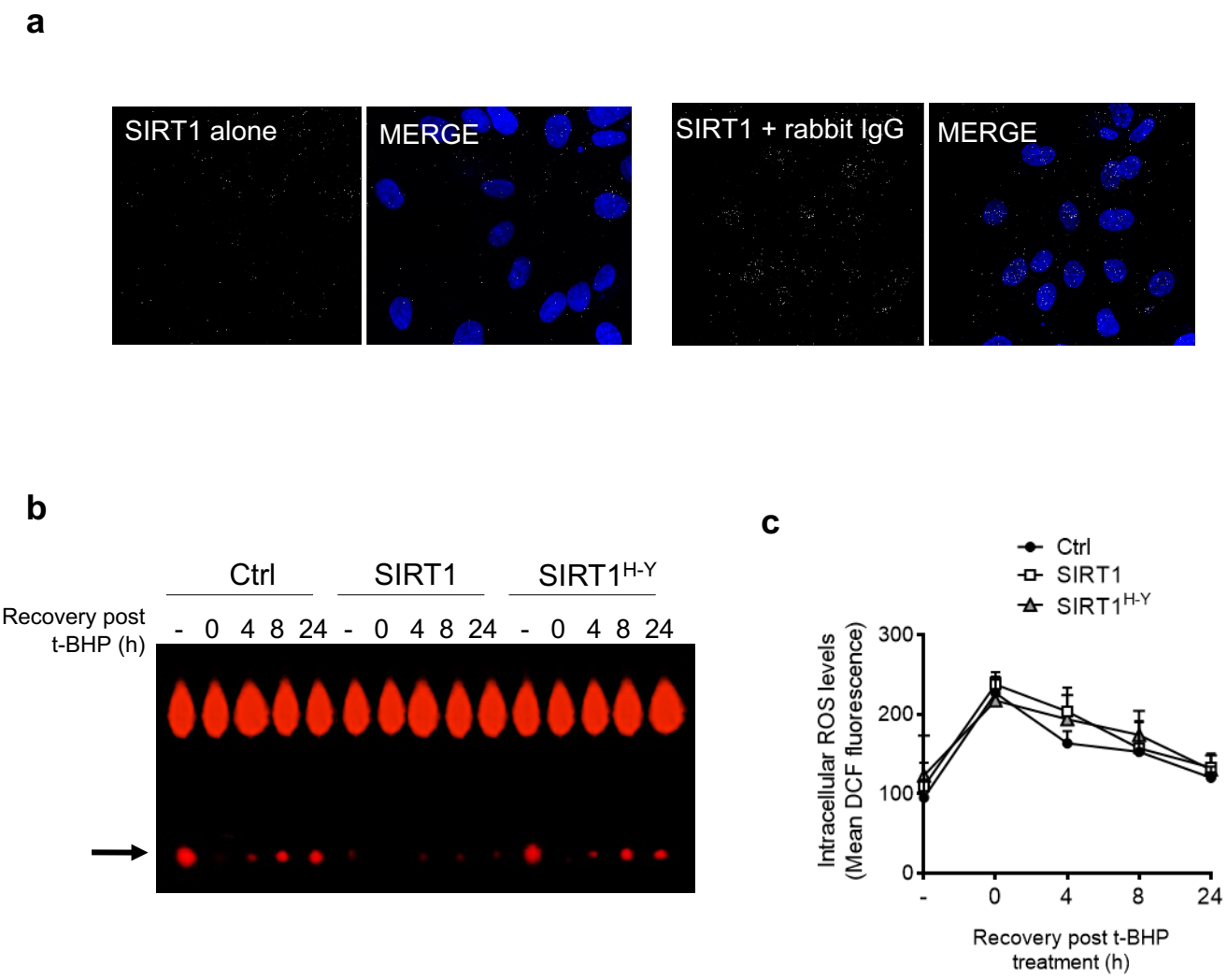

Supplemental Figure V

(a) PLA analysis using mouse anti-SIRT1 antibody alone or with rabbit IgG as negative controls (*n*=3). **(b)** Representative image of BER assay gel showing Ctrl, SIRT1 and SIRT1^{H-Y} cells after 1h t-BHP treatment and 0-24h recovery (*n*=3). **(c)** Quantification of intracellular ROS levels in Ctrl, SIRT1 and SIRT1^{H-Y} VSMCs after 1h t-BHP treatment and 0-24h recovery measured by DCFDA fluorescence (n=3).

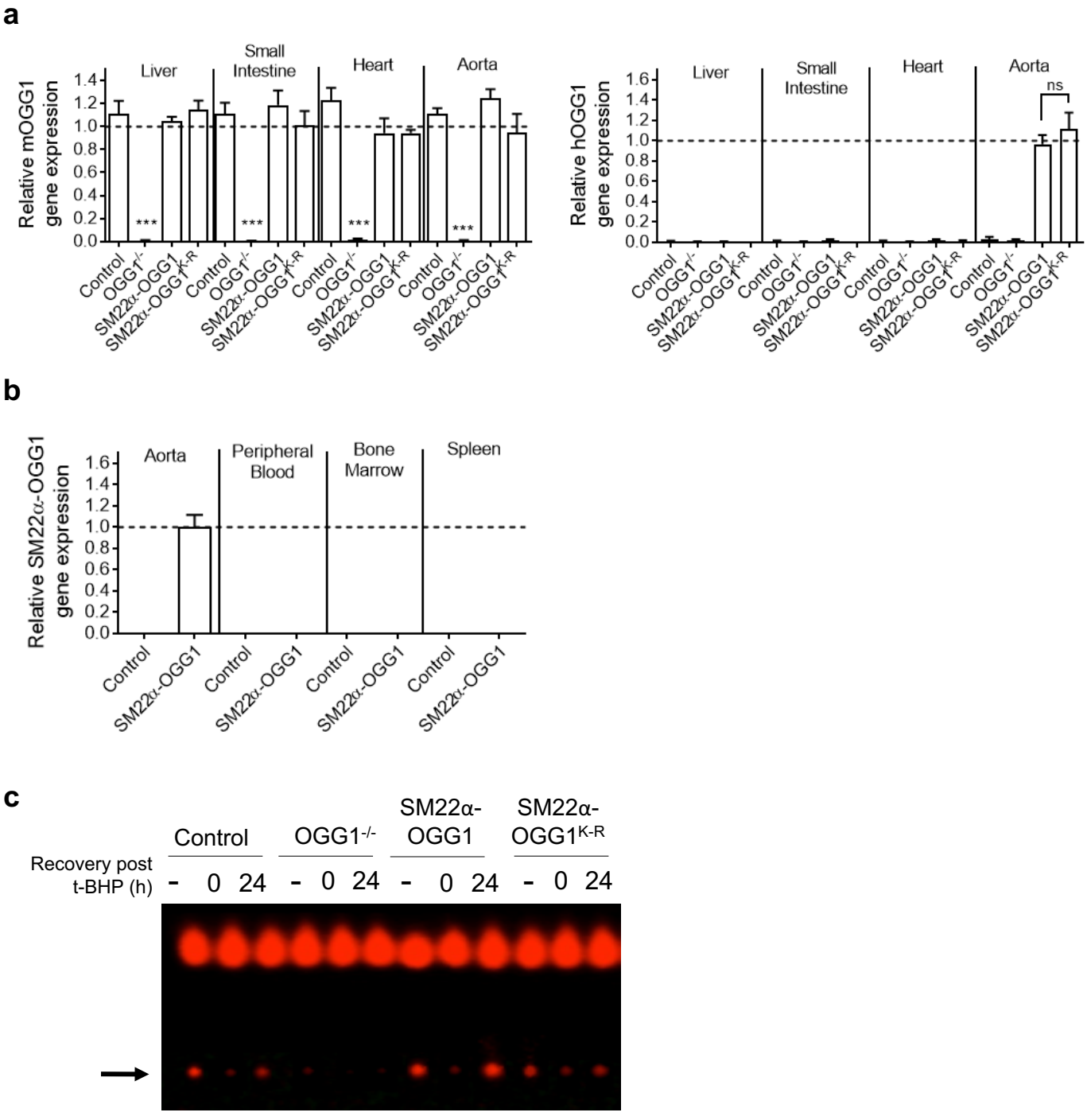

Supplemental Figure VI

(a) qPCR analysis of mouse (mOGG1; left panel) and human (hOGG1; right panel) OGG1 in liver, small intestine, heart and aorta tissue from control, SM22α-OGG1,SM22α-OGG1^{K-R} and OGG1$^{-/-}$ mice (*n*=4). **(b)** qPCR analysis of SM22α-OGG1 in aorta tissue, peripheral blood, bone marrow cells and spleen from control and SM22α-OGG1 mice (*n*=3). **(c)** Representative BER assay in Control, SM22α-OGG1,SM22α-OGG1^{K-R} and OGG1$^{-/-}$ mouse VSMCs after 1h t-BHP treatment and 0-24h recovery (*n*=3). All graphical data are mean ± SEM, ***P< 0.001, one-way ANOVA (Bonferroni post hoc).

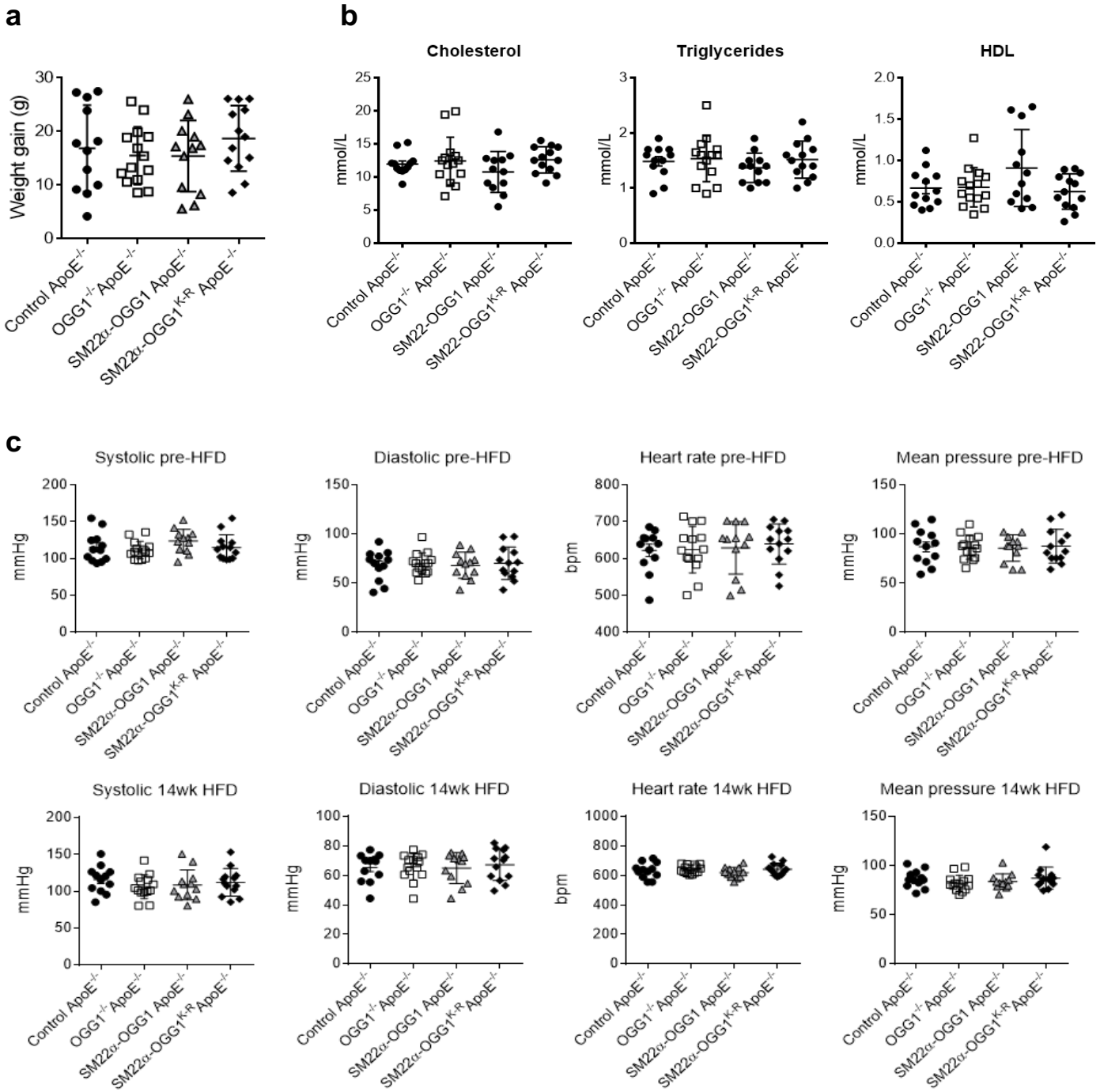

Supplemental Figure VII

(a) Body weight gain, **(b)** serum lipids and **(c)** blood pressure and heart rates in Control ApoE$^{-/-}$ (*n*=12), OGG1$^{-/-}$ ApoE$^{-/-}$ (*n*=14), SM22α-OGG1 ApoE$^{-/-}$ (*n*=12) and SM22α-OGG1$^{K\text{-}R}$ ApoE$^{-/-}$ (*n*=13) mice pre- and post- fat feeding from 8-22 weeks (14w HFD).

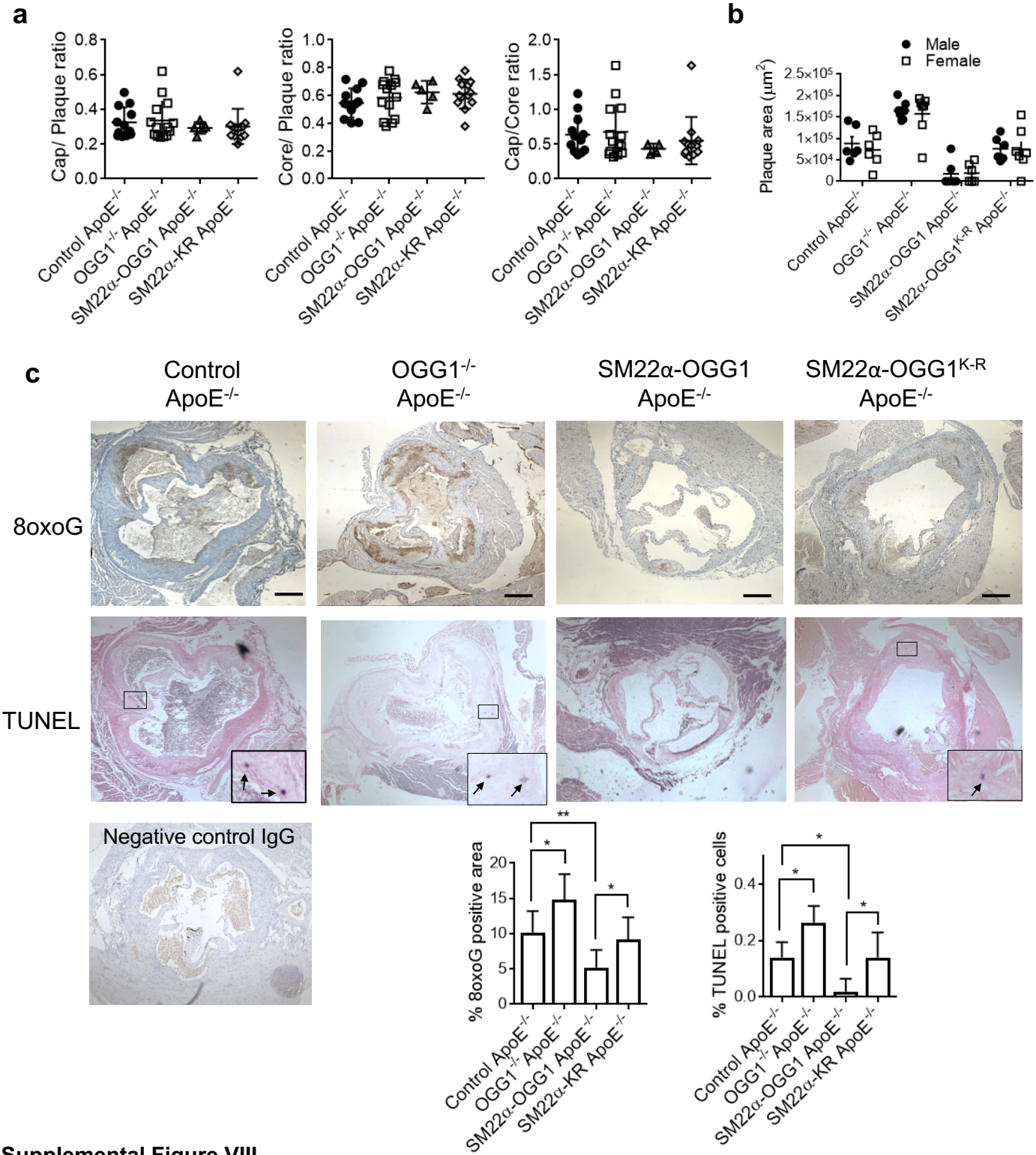

Supplemental Figure VIII

(a) Morphometry of plaques in experimental mice. Quantification of aortic root plaque, core and cap area ratios in control ApoE$^{-/-}$ (n=*12*), OGG1$^{-/-}$/ApoE$^{-/-}$ (n=*14*), SM22α-OGG1/ApoE$^{-/-}$ (n=*5* as caps/cores not discernible in very small lesions) and SM22α-OGG1^{K-R}/ApoE$^{-/-}$(n=*13*) mice at 22 weeks after fat feeding from 8 to 22 weeks (n= 11-14). **(b)** Plaque area of aortic roots in male and female study mice (μm^2). **(c)** 8oxoG and TUNEL immunohistochemistry analysis of Control ApoE$^{-/-}$ (*n*=12), OGG1$^{-/-}$ ApoE$^{-/-}$ (*n*=14), SM22α-OGG1 ApoE$^{-/-}$ (*n*=12) and SM22α-OGG1^{K-R} ApoE$^{-/-}$ (*n*=13) mouse aortic roots at 22 weeks after fat feeding. Negative controls and % 8oxoG-positive aortic area and % TUNEL-positive aortic cells in aortic roots are shown below. All graphical data are mean ± SEM, *P< 0.05, **P<0.01, one-way ANOVA (Bonferroni post hoc).

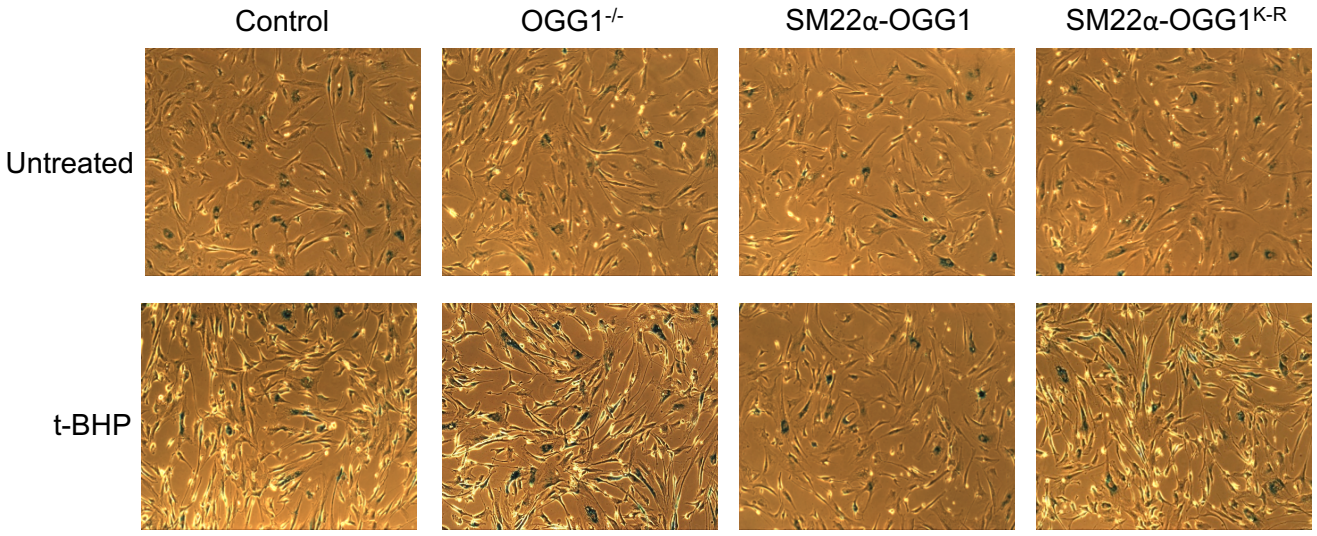

Supplemental Figure IX
Representative images of senescence-associated β-galactosidase activity of VSMCs cultured from Control, OGG1$^{-/-}$, SM22α-OGG1, SM22α-OGG1^{K-R} mice (n=3).

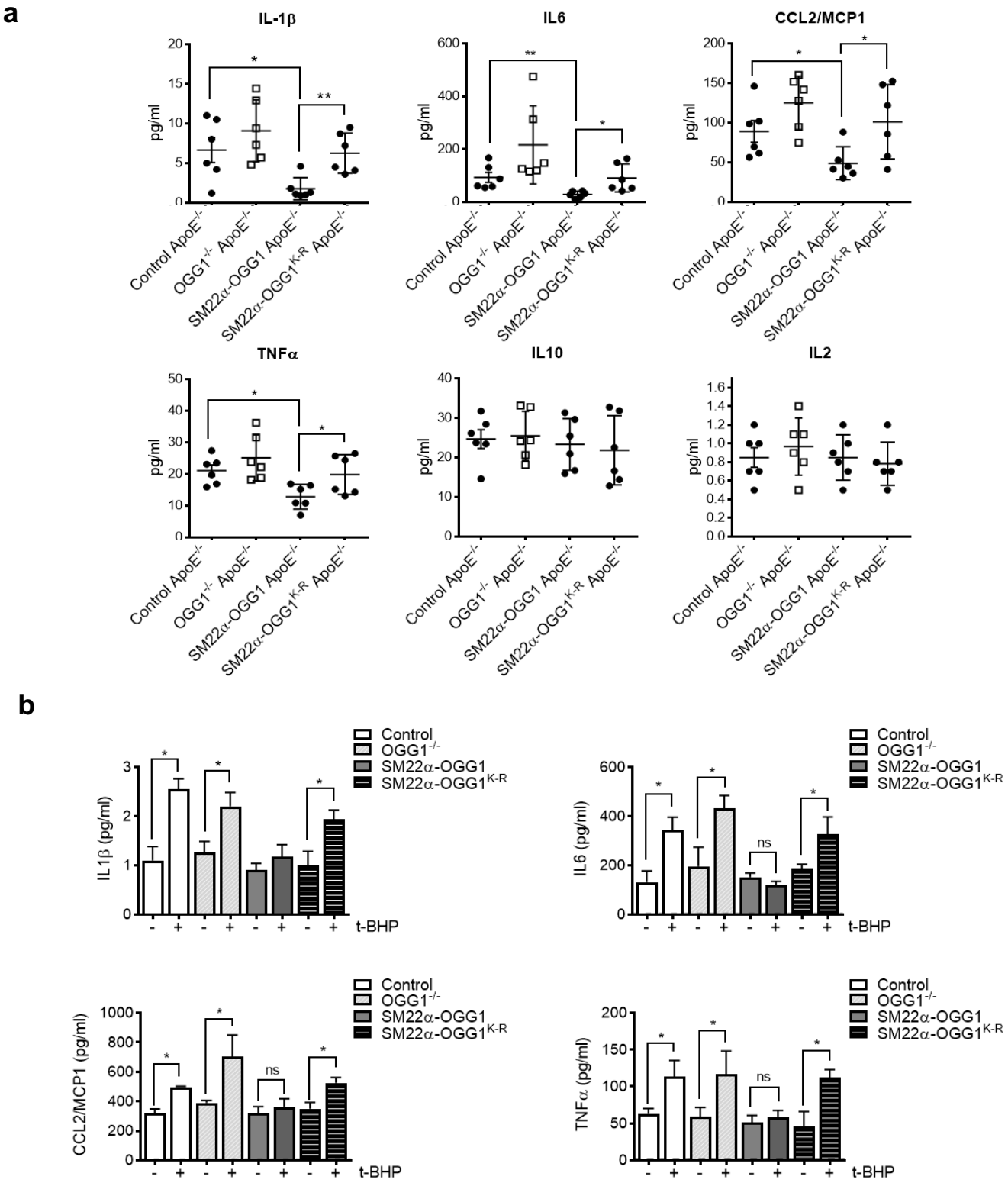

Supplemental Figure X

(a) Serum cytokines from a subset of Control, OGG1$^{-/-}$, SM22α-OGG1, SM22α-OGG1^{K-R} mice at 22 weeks after fat feeding from 8-22 weeks (n=*6*). **(b)** Levels of CCL2/MCP1, IL1β, IL2, IL6, IL10 and TNFα in conditioned media from experimental mouse VSMC cultures stimulated with t-BHP measured by multiplex ELISA (n=3), Student's t-test. All graphical data are mean ± SEM, *P < 0.05, **P < 0.01, one-way ANOVA (Bonferroni post hoc).